# Exhuming an Accretionary Prism: A Case Study of the Kodiak Accretionary Complex, Alaska, USA

Kristijan Rajič, Hugues Raimbourg, Vincent Famin, Benjamin Moris-muttoni, Donald M Fisher, Kristin D Morell, Aurélien Canizarés

Tectonics

RESEARCH ARTICLE
10.1029/2023TC007754

# Exhuming an Accretionary Prism: A Case Study of the Kodiak Accretionary Complex, Alaska, USA

**Kristijan Rajič[1], Hugues Raimbourg[1], Vincent Famin[2,3], Benjamin Moris-Muttoni[1], Donald M. Fisher[4], Kristin D. Morell[5], and Aurélien Canizarés[6]**

[1]Institut des Sciences de la Terre d'Orléans, Université d'Orléans/CNRS/BRGM UMR7327, Orléans, France, [2]Laboratoire GéoSciences Réunion, Université de La Réunion, Saint-Denis, France, [3]Institut de Physique du Globe de Paris, CNRS, UMR 7154, Université de Paris, Paris, France, [4]Department of Geosciences, Pennsylvania State University, University Park, PA, USA, [5]Department of Earth Science, University of California, Santa Barbara, Santa Barbara, CA, USA, [6]CNRS, CEMHTI UPR3079, University Orléans, Orléans, France

**Abstract** We have carried a structural study across Kodiak accretionary complex in Alaska, USA, in order to describe its thermal structure and decipher the processes of exhumation. The accretionary complex consists of a stack of tectonic mélanges and coherent units. Mélanges are characterized by simple shear deformation with a pervasive network of top-to-the-trench shear zones, whereas coherent units are affected principally by horizontal shortening, except for spatially limited outcrops in Kodiak Central Belt. Peak temperatures estimated using Raman spectroscopy of carbonaceous material range from 220 to 400°C through most of the complex. These temperatures coincide with estimates from metamorphic parageneses and are interpreted as temperatures of deformation achieved under a high gradient due to contemporaneous ridge subduction. The highest temperatures are recorded in the central part of the complex, pointing to a dome-like structure. Lower temperatures (~120°C) are recorded along the southeastern border of the complex, in slope sediments unconformably overlying accreted units. Based on the combination of structural and thermal data, we conclude that the rocks constituting the Kodiak complex experienced at least two stages of burial and then exhumation, with vertical motions reaching up to ~13 km from the Paleocene to the present. Given the pervasive horizontal shortening within the wedge, exhumation resulted from prism thickening contemporaneous with surficial erosion. Recorded subsidence episodes may be local phenomena associated with thrusting or large-scale processes associated with basal erosion. The rates of vertical motion range from 0.2 to 1.3 mm/yr, comparable with estimates in modern margins.

**Plain Language Summary** In this study, we examined several units from the Kodiak accretionary complex, an archetypal example of the accretionary wedge in southern Alaska, to improve our understanding of the processes that influence convergent margins. These units were subducted to significant depths, but the mechanisms responsible for their exhumation back to the surface remain unclear. Estimated peak-burial temperatures in basally accreted units across the complex are in the range 220–400°C, with a temperature gap between basally accreted units and slope sediments (100–140°C). Temperatures and pressures suggest a burial down to depths of ~7–13 km. Based on deformation kinematics and temperature estimates in basally accreted units and slope sediments, we propose that the exhumation periods result from basal accretion, horizontal shortening, and surficial erosion. In contrast, subsidence most likely resulted from thrusting in the upper plate or basal erosion.

**Key Points:**

- A maximum temperature of the order of 300–400°C is observed in the central part of the complex, decreasing to ~220–300°C landward and seaward
- The accretionary complex experienced two sequences of rock burial and then exhumation since the Paleocene
- Exhumation at rates of ~0.2–1.3 mm/yr resulted from uplift associated with surficial erosion

**Supporting Information:**

Supporting Information may be found in the online version of this article.

**Correspondence to:**

K. Rajič,
kristijan.rajic@univ-orleans.fr

**Citation:**

Rajič, K., Raimbourg, H., Famin, V., Moris-Muttoni, B., Fisher, D. M., Morell, K. D., & Canizarés, A. (2023). Exhuming an accretionary prism: A case study of the Kodiak accretionary complex, Alaska, USA. *Tectonics*, *42*, e2023TC007754. https://doi.org/10.1029/2023TC007754

Received 11 JAN 2023
Accepted 27 SEP 2023

**Author Contributions:**

**Conceptualization:** Hugues Raimbourg, Vincent Famin
**Data curation:** Kristijan Rajič, Benjamin Moris-Muttoni
**Formal analysis:** Kristijan Rajič, Aurélien Canizarés
**Funding acquisition:** Hugues Raimbourg, Vincent Famin
**Investigation:** Kristijan Rajič, Vincent Famin, Donald M. Fisher, Kristin D. Morell, Aurélien Canizarés
**Methodology:** Kristijan Rajič, Hugues Raimbourg, Benjamin Moris-Muttoni, Aurélien Canizarés
**Project Administration:** Hugues Raimbourg, Vincent Famin



## 1. Introduction

Seismic reflection profiles, deep sea drilling, and geodynamic models suggest that sedimentary rocks from the subducting plate are transferred to the upper plate principally by two processes. In the first process, the propagation of in-sequence, landward-dipping thrusts leads to frontal accretion of sediments at the trench (e.g., Dahlen, 1990; Davis et al., 1983; Menant et al., 2020; Moore, 1989; Moore et al., 1990, 2001; Pajang et al., 2021). In the second process, wedge thickness increases by underplating of coherent units and mélanges below the wedge (e.g., Byrne & Fisher, 1987; D. M. Fisher & Byrne, 1987; Platt, 1986; Sample & Fisher, 1986). Concurrent with these two mechanisms of burial, the exhumation of underplated lithologies back to the surface also occurs within accretionary wedges, which may rely on the operation of several distinct processes. In the conceptual framework of the critical wedge (Dahlen, 1984, 1990), as more material is underplated, the wedge thickens, and the surface

**Resources:** Hugues Raimbourg, Donald M. Fisher, Kristin D. Morell
**Software:** Kristijan Rajič, Benjamin Moris-Muttoni, Aurélien Canizarés
**Supervision:** Hugues Raimbourg
**Validation:** Hugues Raimbourg
**Visualization:** Kristijan Rajič
**Writing – original draft:** Kristijan Rajič, Hugues Raimbourg, Vincent Famin
**Writing – review & editing:** Hugues Raimbourg, Benjamin Moris-Muttoni, Donald M. Fisher, Kristin D. Morell, Aurélien Canizarés

slope increases until reaching a critical taper angle. Then, further growth of the wedge by basal underplating is counterbalanced by horizontal extension and normal faulting, which contribute to exhumation. In parallel, surficial erosion can remove the rock overburden and further contribute to exhuming deeper levels of the accretionary wedge (Platt, 1986; Ring et al., 1999).

Exhumed fossil subduction zones provide additional information about the tectonics active on the plate boundary and within the wedge. Accretionary complexes, such as the Shimanto Belt of Japan or the Franciscan Complex in North America, are characterized by either mélanges or coherent units that experienced non-coaxial deformation due to intensive shearing along or near plate-boundary interface (e.g., Fagereng & Sibson, 2010; Meneghini et al., 2009; Raimbourg et al., 2019). The subsequent deformation that occurs after the incorporation of material into the wedge is often strongly localized along out-of-sequence thrust faults and their associated damage zones (e.g., D. M. Fisher & Byrne, 1987; Kondo et al., 2005; Rowe et al., 2009; Smeraglia et al., 2019). These contractional structures produce prism thickening, but the removal of overburden from above the underplated rocks requires an exhumation mechanism.

The Kodiak accretionary complex represents a well-described and exposed paleo-accretionary complex that lies in the forearc of the active Alaskan margin (Byrne & Fisher, 1987; Plafker et al., 1994). This complex is part of one of the largest accretionary prisms worldwide, extending from the Sanak Islands in the west to the Alexander Archipelago to the east, and is bordered to the north by the Wrangellia composite terrane along the Border Ranges Fault System (Plafker et al., 1994). The complex consists of trench-parallel striking metaturbidites and metamafic units, which, before exhumation, experienced subduction-related and intra-wedge deformation during multiple phases of accretion (Byrne & Fisher, 1987). Therefore, the record of this complex allows for the investigation of long-lived rock history, including accretion, burial, and exhumation. Herein, the Kodiak accretionary complex was analyzed to study the timing, rates, and amounts of exhumation.

In this work, we report the results of an extensive field survey across the Kodiak accretionary complex to unravel variations in deformation and thermal history from the Cretaceous to the present. First, we describe, in each unit, deformation structures and kinematics to determine whether it occurred during underthrusting along the plate-boundary interface or after incorporation into the wedge. Then, we reconstruct the thermal/burial history of the complex by applying Raman spectroscopy of carbonaceous material (RSCM) along the studied profile. Finally, we use a combination of observed deformation structures, paleotemperature results, previously published stratigraphic ages, geochronology, and low-temperature thermochronometric results to show that accreted rocks underwent different stages of exhumation/burial. We conclude by discussing conceptual models for rock exhumation/burial within global accretionary complexes.

## 2. The Anatomy of the Kodiak Accretionary Complex

The sedimentary terranes that form the Kodiak paleo-accretionary prism range from Jurassic metamorphic rocks exposed on the northwestern side of the archipelago to the youngest Miocene units on the southeast coast (Byrne & Fisher, 1987; Connelly, 1978; Moore et al., 1983; Roeske et al., 1989; Sample & Moore, 1987). The metamorphic grade parallels the age of the rocks (Figure 1). From northwest to southeast, the rocks evolve from: (a) blue- and greenschist facies at the northwestern Jurassic Raspberry Schist (Roeske et al., 1989), (b) to prehnite-pumpellyite and greenschist in the Cretaceous-Early Paleocene Uyak Complex, Kodiak and Ghost Rocks Formation (Brantley & Fisher, 1997; Connelly, 1978; Sample & Moore, 1987; Vrolijk et al., 1988), (c) and finally to the zeolite facies and mildly deformed sedimentary rocks of the Eocene-Miocene Sitkalidak, Sitkinak, and Narrow Cape Formations (Moore & Allwardt, 1980; Moore et al., 1983).

The Uyak Complex is described as a tectonic mélange with block-in-matrix texture characterized by lenses of greywacke, chert, mafic rocks, tuff, and limestones within sheared argillitic layers (Connelly, 1978). Stratigraphic ages from the Uyak Complex indicate that it was deposited on top of the oceanic plate through the Jurassic up to the Early Cretaceous (Clift et al., 2005; Connelly, 1978; Pavlis et al., 1988). The Uyak Complex was deformed by underthrusting between the Valanginian and the Maastrichtian (Connelly, 1978). The metamorphic conditions recorded in basalt lenses in this unit reach up to the prehnite-pumpellyite facies (Connelly, 1978). Fluid inclusion studies in extensional veins formed during underthrusting document a trapping temperature of 270–290°C and pressure of 3.3 kbar (Vrolijk et al., 1988). The Uyak Complex is in tectonic contact with the Kodiak Formation along the Uganik Thrust (Moore, 1978; Rowe et al., 2009; Figure 1).

10.1029/2023TC007754



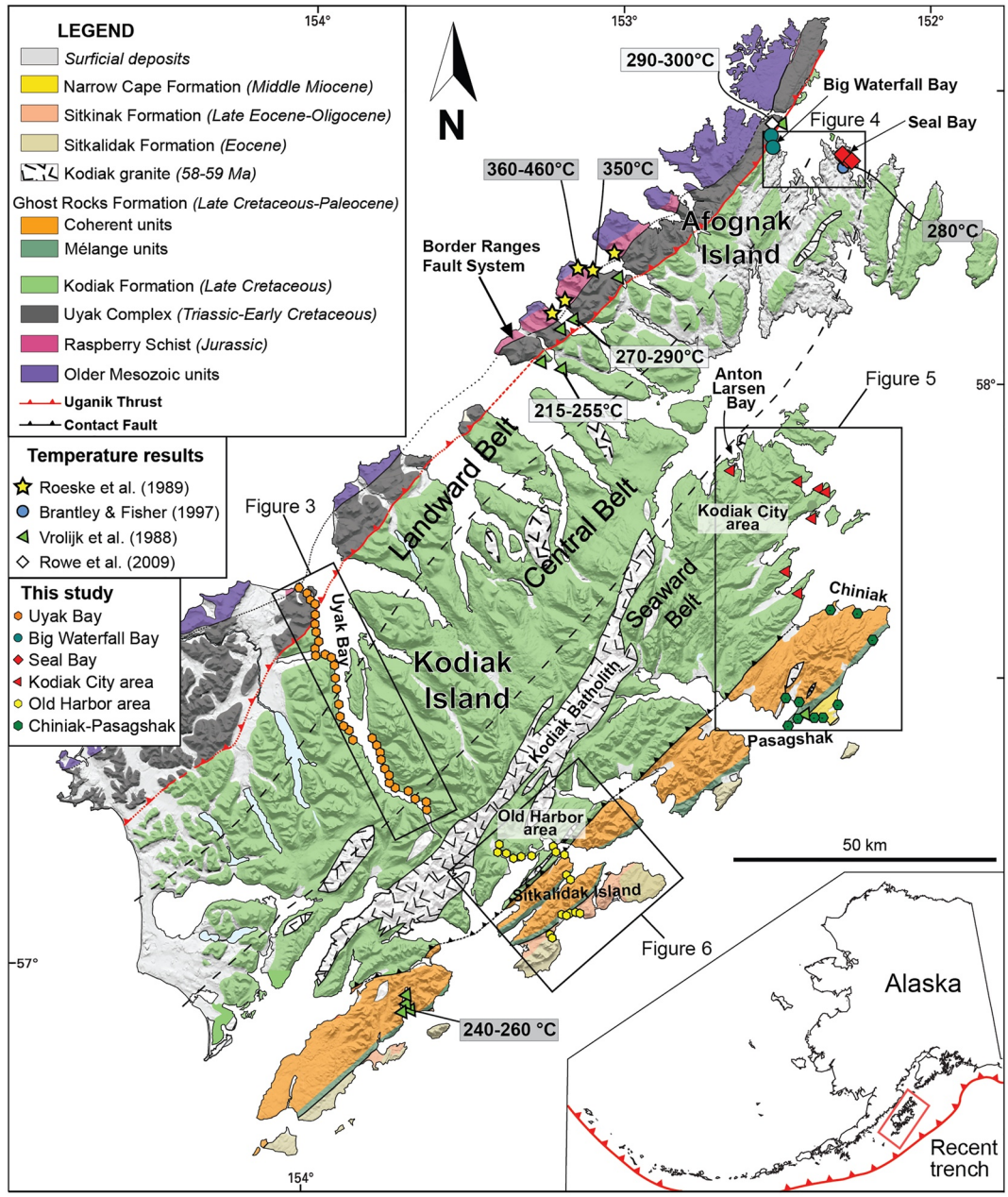


**Figure 1.** Geological map of the Kodiak archipelago modified after Wilson et al. (2005) with previously published temperature results. Dashed lines in the Kodiak Formation are estimated borders between the Landward, Central, and Seaward Belts.

The Kodiak Formation is a sequence of turbidites—slates, siltstones, and sandstones—interpreted as oceanic trench sediments accumulated during the Late Cretaceous (Byrne & Fisher, 1987). The age of sedimentation is determined as Maastrichtian (~70 Ma) by the occurrence of *Inoceramus kusiroensis* (Byrne & Fisher, 1987). The dominant deformation structure in the Kodiak Formation is a slaty cleavage. Based on the orientation of this slaty cleavage, Sample & Moore (1987) subdivided the Kodiak Formation into a Landward Belt (with a northwest-dipping slaty cleavage), a Central Belt (sub-horizontal cleavage) and a Seaward Belt (northwest-dipping cleavage; Figure 1). Vitrinite reflectance in the Kodiak Formation has an average value of 3.73, suggesting a temperature of ~225°C (Sample & Moore, 1987). Based on cogenetic $CH_4$- and $H_2O$-rich fluid inclusions from syn-cleavage quartz veins in the Landward Belt, minimum temperatures and pressures are estimated as 215–250°C and 2.8 kbar, respectively (Myers & Vrolijk, 1986). At Seal Bay, where the Kodiak Central Belt is

exposed, an average temperature of 280°C was obtained using $\delta^{18}O$ thermometry on quartz, mica, and chlorite (Brantley & Fisher, 1997). The Contact Fault separates the Kodiak Formation to the northwest from the Ghost Rocks Formation to the southeast (Farris, 2010).

Dominant lithologies in the Ghost Rocks Formation are shale and sandstone, with minor conglomerate, volcanic rock, and limestone (Byrne, 1982; Moore, 1989). Pelagic foraminifera from limestone indicate a Late Cretaceous-Early Paleogene age (Moore et al., 1983 and references therein). The southeastern part of the Ghost Rocks Formation is described as a tectonic mélange, named the Ghost Rocks Mélange, whereas the northwestern part is represented as a coherent portion of the unit (Byrne, 1982). Vitrinite reflectance ($R_0$) on samples from the Ghost Rocks Formation ranges from 2.15% to 2.95%, suggesting the peak temperatures of 225–250°C (Moore et al., 1983). The minimum temperature estimated by fluid inclusion studies from syn-tectonic extensional veins at Jap Bay and the Pasagshak area is 250 ± 20°C, with a trapping pressure of ∼3 kbar (Vrolijk et al., 1988).

The Kodiak and the Ghost Rocks Formations were intruded by andesite and granodiorite plutons, dated at 58–59 Ma by U-Pb analysis of monazite and zircon (Farris et al., 2006). Such plutons, among which the Kodiak Batholith is the largest, are interpreted as being formed during ridge subduction and the interaction of MORB-like magmas with sedimentary rocks in the prism (Farris, 2010; Farris et al., 2006; Moore et al., 1983). It is proposed that both the Kodiak Formation and the Ghost Rocks Formation were accreted prior to ridge subduction (Byrne & Fisher, 1987; Sample & Fisher, 1986; Sample & Moore, 1987).

The Sitkalidak Formation, exposed along the southeast side of the archipelago, consists of sandstone and shale layers (Byrne & Fisher, 1987; Moore & Allwardt, 1980; Moore et al., 1983). The sedimentation age of the Sitkalidak Formation is determined as Eocene (Moore & Allwardt, 1980; Moore et al., 1983). Unlike all other units, it contains abundant thrust faults with landward vergence (Moore & Allwardt, 1980). Based on vitrinite reflectance results, Moore and Allwardt (1980) proposed that the Sitkalidak Formation experienced a peak temperature of 100–125°C.

Along the southeast margin of the Kodiak archipelago, Tertiary sediments in slope basins overlie the Ghost Rocks Formation and Sitkalidak Formation along angular unconformities. For example, the nonmarine to shallow marine sediments of the Oligocene Sitkinak Formation unconformably overlies the Sitkalidak Formation (Moore & Allwardt, 1980 and references therein), and Middle Miocene shallow water sediments of the Narrow Cape Formation unconformably overlie the Ghost Rocks Formation (Moore et al., 1983). The metamorphic temperatures inferred for the Sitkinak Formation from vitrinite reflectance range from 100 to 125°C (Moore & Allwardt, 1980).

## 3. Methodology

### 3.1. Kinematic Analysis of Deformation Structures

The attitude of micro- and meso-structures was measured in the field and used to reconstruct the deformation history of the accretionary prism. Bedding or foliations were measured at each site together with deformation structures. Structures include kinematic indicators (such as meter-scale striated faults, shear bands, fractures, or dykes and extension fractures typically filled with syn-deformation minerals) and indicators of finite strain (foliation, crenulation cleavage, and fold axes). The measured data were processed following the recommendations of Delvaux and Sperner (2003) and Sperner & Zweigel (2010), which include the search for chronological relationships in the field, the attribution of a confidence level to each datum (certain, probable, supposed, unknown), and the user-driven separation of data into mechanically compatible subsets. Structural data were manually sorted according first to their crosscutting relationships and then to their kinematics and orientation.

We limited our kinematic analysis to the determination of shortening (P), intermediate (B), and extension (T) axes of the deformation ellipsoid. The kinematic analysis was performed using the PBT method of the WinTensor program (Delvaux et al., 2013), which determines the statistical distribution of kinematic axes for a given subset of data.

### 3.2. Raman Spectroscopy of Carbonaceous Material

From each locality where deformation structures were studied, a thick (200 μm) section oriented in the X-Z plane of the kinematic referential was prepared from metasedimentary samples for RSCM. Wherever magmatic rocks

were present, for instance, at several localities in the Ghost Rocks Formation and Uyak Complex, samples for RSCM were chosen at least a few meters away from the boundary of the pluton to avoid any effect of contact metamorphism. In the prepared thick sections, analyzed particles were chosen away from any shear bands to avoid shear-enhanced thermal maturation of the carbonaceous material (e.g., Petroccia et al., 2022).

We performed RSCM using a Raman Renishaw InVia Reflex micro-spectrometer at the ISTO-BRGM and Renishaw InVia Qontor micro-spectrometer at CEMHTI CNRS, Orléans. The silicon standard was used for the calibration. The light source was a 514.5 nm Ar laser with a power of about 1 mV, focused by a Leica DM2500 microscope at the magnification of 100X. The signal was analyzed by a CCD NIR/UV detector. 15–20 points were analyzed per sample on 150–200 μm polished thick sections. To avoid defect bands generated during the preparation of the thin sections, particularly polishing, all analyses were performed on subsurface grains by focusing the laser beam through transparent minerals, generally quartz (Ammar & Rouzaud, 2012; Katagiri et al., 1988; Pasteris, 1989). Raman spectra contain two main defect bands, so-called D1 (at ∼1,350 $cm^{-1}$) and G (at ∼1,580 $cm^{-1}$) bands, with three additional defect bands (D2 band at ∼1,620 $cm^{-1}$, D3 band at ∼1,500 $cm^{-1}$, and D4 band at ∼1,200 $cm^{-1}$), whose presence or absence is related directly to experienced peak-metamorphic temperatures (Beyssac et al., 2002; Lahfid et al., 2010). The final deconvolution was made according to the method of Lahfid et al. (2010) or Beyssac et al. (2002) according to the following criteria: (a) If a D4 band was present together with a relatively high D3 and small D2 bands, the Lahfid et al. (2010) method was applied. Raman spectra were processed with the software PeakFit 4.12 by subtracting the baseline and fitting the obtained spectrum with five Lorenzian bands. From the area below five Lorenzian bands, a RA1 ratio was calculated using the equation RA1 = (D1 + D4)/(D1 + D2 + D3 + D4 + G). The final temperature was estimated following equation T (°C) = 1,250 × RA1 − 469.75 (Lahfid et al., 2010). (b) If the Raman spectra contained an obvious D2 band, a low D3 band, and an absent D4 band, the deconvolution process was made according to Beyssac et al. (2002) procedure. Three Voight functions were applied to estimate the area, from where the R2 ratio was calculated by the equation R2 = D1/(D1 + G + D2). The peak temperature was calculated following equation T (°C) = −445 × R2 + 641.

In five samples from the Sitkinak Formation and three samples from the Narrow Cape Formation, the Raman spectrum were processed following the method by Schito et al. (2017) since the method by Lahfid et al. (2010) is invalid below 200°C. After subtracting the baseline and applying six mixed Gaussian-Lorentzian bands, an RA2 ratio was calculated from the areas by the equation RA2 = (S + DI + D)/(Dr + GI + G). Finally, an RA2 value was correlated with Vitrinite Reflectance VR% (Schito et al., 2016), for which the linear correlation between RA2 and VR% was found (Schito et al., 2017). The method is modeled with the geothermal gradient of 38°C/km (Schito et al., 2016, 2017), which is similar to the estimated paleogeothermal gradient of ∼30°C/km in the Sitkalidak and Sitkinak Formations during the Miocene (Moore & Allwardt, 1980).

## 4. Results

### 4.1. Deformation Structures

The following section describes deformation structures in accreted coherent units, tectonic mélanges, slope sediments, and across large-scale faults. Structural data and analysis for each locality used in this study are presented in Table S1.

#### 4.1.1. Accreted Units

##### *4.1.1.1. Coherent Units*

Based on variations in deformation style and dip angles of bedding stratification and slaty cleavage, coherent units can be divided into three distinct zones, roughly following the subdivision as the Landward, Central, and Seaward Belt (as proposed by Sample and Moore (1987)). The Kodiak Seaward Belt and the coherent part of the Ghost Rocks Formation are grouped together due to similarities in deformation structures.

The most northwestern part of the Kodiak Formation, the Landward Belt, is characterized by a relatively steep (∼50–60°) northwest-dipping bedding stratification and slaty cleavage. The main deformation structures are top-to-the-SE shear bands (Figure 2a), pointing to non-coaxial deformation. This type of deformation is limited to a few hundreds of m near the Uganik Thrust (Sites 19KO17 and 22KO24 in Uyak Bay; Site 19KO27 in Big Waterfall Bay).

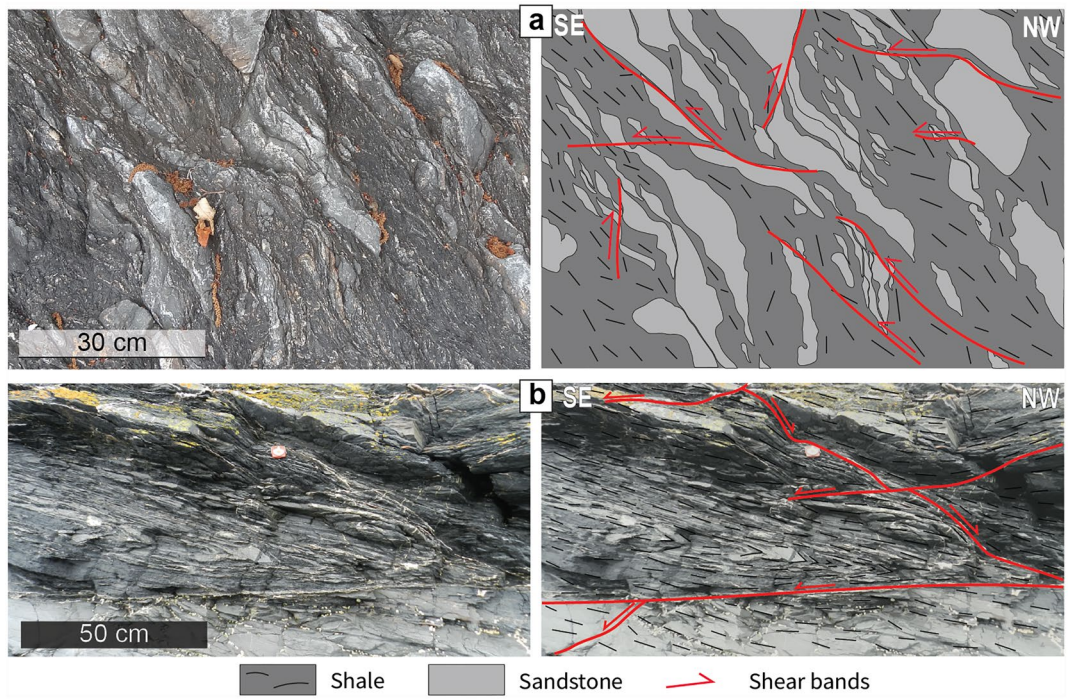


**Figure 2.** Deformation structures in the inner part of the Kodiak Formation: (a) Top-to-the-trench shear bands in the Kodiak Landward Belt (Site 19KO17). (b) Conjugate extensional shear bands filled with quartz, Uyak Bay (Site 22KO16).

Further toward the southeast in the Kodiak Formation, in Uyak and Seal Bays, the bedding stratification and slaty cleavage dip toward the northwest but at a lower angle than in the Landward Belt. A pervasive slaty cleavage is observed at a low angle to the bedding stratification (Figure 3). The Kodiak Formation in Seal Bay is characterized by low-angle slaty cleavage and bedding stratification (Figure 4). Most of the observed shear bands at Seal Bay show a normal sense of shear (Figure 2b). Once the slaty cleavage is rotated to the horizontal position these shear bands become a set of conjugate extensional shear bands, which corresponds to horizontal extension in their present-day attitude (Figure 2b). These shear bands are made up of quartz and to a lesser extent calcite. Also, sub-vertical NE-striking quartz veins have been observed, often forming en échelon arrays, mainly dipping toward the southeast or, to a lesser extent, to the northwest.

In the Kodiak Seaward Belt (Kodiak City and Old Harbor areas) and Ghost Rocks Formation (Chiniak area and Sitkalidak Island), bedding is sub-vertical with a dip direction dominantly to the northwest (Figures 5 and 6). The sub-vertical slaty cleavage is well developed and at a low angle (20–40°) with bedding. Common structures include conjugate sets of NW-and SE-dipping reverse shear bands filled with quartz fibers (Figures 5a, 5b, and 6a). These conjugate shear bands are up to 5 m long and often form anastomosing networks (Figure 7a). Other frequently observed structures are strike-slip, dominantly dextral faults (Figures 5a, 5b, 6a, and 7b). Isoclinal folds indicating horizontal NW-SE shortening were found occasionally throughout the frontal part of the complex (Figure 7c).

Within the granite pluton of Anton Larsen Bay, strike-slip faults are also observed, but most are sinistral (Figure 5f), contrary to other sites in the Seaward Belt and Ghost Rocks Formation.

#### *4.1.1.2. Mélange Units*

The tectonic mélange units, including the Uyak Complex and Ghost Rocks Mélange, show a similar deformation style and distinct from the accreted coherent units. Both mélanges are characterized by a dominantly non-coaxial deformation.

In the Uyak Complex, basalts, cherts, and sandstone lenses are boudinaged and embedded within strongly sheared shale. Basalt phacoids show a penetrative foliation and locally a lineation (average 47/313). NW-dipping shear bands with a top-to-the-SE sense of shear are the dominant deformation structures (Figures 3 and 8a), either filled

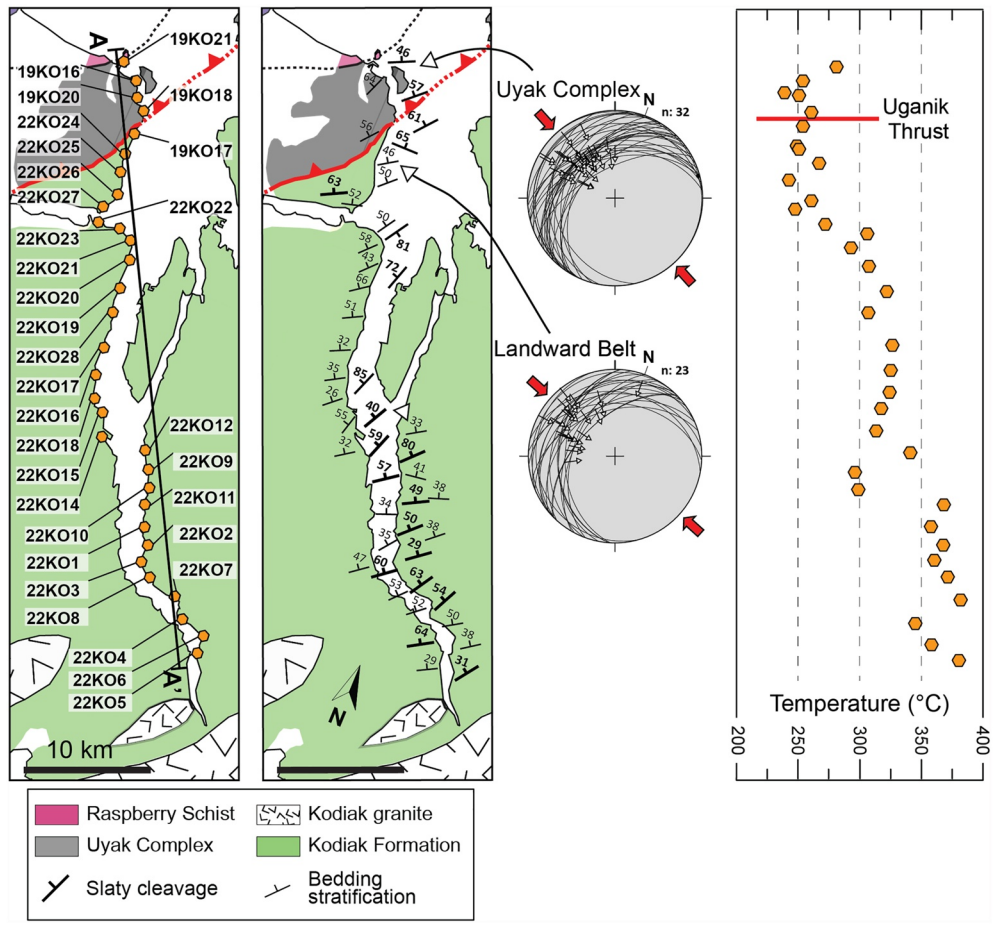


**Figure 3.** Geological map of Uyak Bay with locations of samples, stereonets of bedding, slaty cleavage, representative deformation structures (equal area, lower hemisphere), and Raman spectroscopy of carbonaceous material temperature profile. The upper pole figure represents top-to-the-SE shear bands in the Uyak Complex, whereas the lower shows top-to-the-SE shear bands in the Kodiak Landward Belt close to the Uganik Thrust.

with quartz or unmineralized. Boudinaged chert layers often contain Mode 1 quartz veins located in the neck of the boudins.

The Ghost Rocks Mélange in the Pasagshak area is characterized by a block-in-matrix texture made of sandstone and basalt boudins embedded in a shale matrix. Bedding and foliation are oriented on average 43/293 and 06/322, respectively. Most thrust faults dip to the northwest (average 45/312) with a top-to-the-SE sense of shear. In contrast, a minority of faults exhibit a southeast dip (Figure 8b) and a top-to-the-NW sense of shear (Figure 5e). As in the case of the Ghost Rocks Formation and the Kodiak Seaward Belt, NE- and NW-striking strike-slip faults are observed, with mostly dextral slip (Figure 5e).

### 4.1.2. Slope Sediments

#### *4.1.2.1. Sitkinak Formation*

The Oligocene Sitkinak Formation is nicely exposed at the southern part of Sitkalidak Island. Bedding is sub-vertical, 83/344 on average, with slight variations in strike, from W-E to NE-SW. A weak slaty cleavage is also observed, oriented 85/322 on average (Figure 6). Thrust faults are dominantly characterized by a southward dip and a northward vergence, and a smaller number of faults have a northward dip and a southward vergence (Figure 9b). These two groups of faults form a conjugate set of thrust faults (Figure 6b).

#### *4.1.2.2. Narrow Cape Formation*

Middle Miocene sediments of the Narrow Cape Formation, deposited above an unconformity on top of the Ghost Rocks Formation, are characterized by different bedding attitudes (Figure 5; 25/323, 26/164, and 36/344 for sites

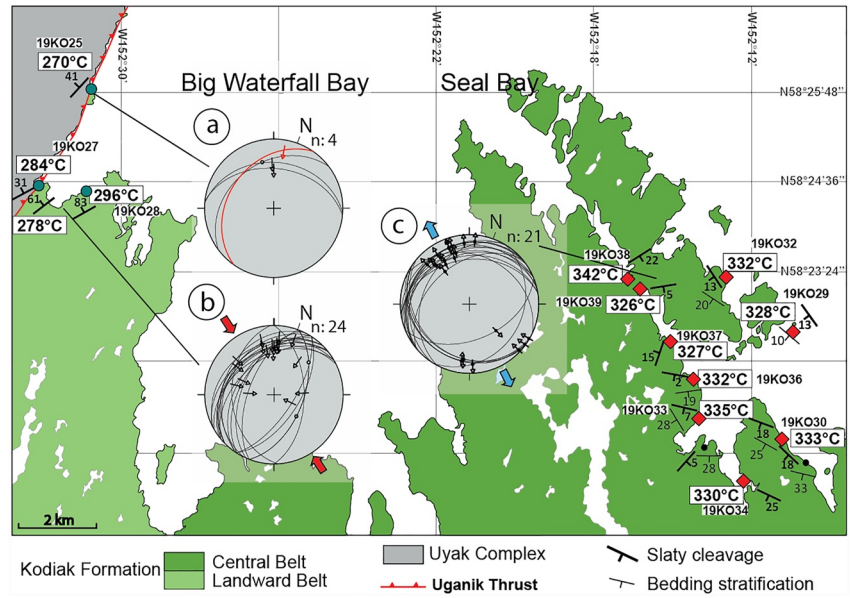


**Figure 4.** Map of Seal Bay and Big Waterfall Bay with estimated Raman spectroscopy of carbonaceous material temperatures and stereonets of stratification bedding and slaty cleavage (equal area, lower hemisphere). Stereographic plots: (a) Shear bands in the damage zone of the Uganik Thrust (black) and the thrust plane itself (red). (b) Shear bands from the Kodiak Landward Belt 1 km away from the Uganik Thrust. (c) Extensional shear bands from the Kodiak Central Belt indicate an SE-NW extension.

19KO08, 19KO15, and 22KO48, respectively). Deformation is relatively discrete, and deformation structures include calcite-filled, m-scale normal and thrust faults with similar strikes and opposing dips (Figure 9a). At site 19KO08, both types of faults have NW-dips, whereas, at site 19KO15, they have SE-dips. After the restoration of bedding back to horizontal at both sites, these faults become conjugate thrust faults (Figure 5g).

#### 4.1.3. Large-Scale Faults

At Big Waterfall Bay, the fault core of the Uganik Thrust is characterized by a 0.15–0.30 m thick cataclastic zone in the footwall belonging to the Kodiak Landward Belt and a 1–2 m thick mylonite in the hanging wall belonging to the Uyak Complex (Figure 10a). A thick (few meters) damage zone is observed in the footwall bellow the cataclastic zone (Figure 10b). The fault plane bordering the cataclastic zone is oriented 34/305, with a slickenline plunging toward N170 and with top-to-the-trench sense of shear. Asymmetric folds within the hanging wall mylonite confirm this thrust sense of motion (Figure 10c; for more details, see Rowe et al., 2009). The mylonite in the hanging wall is cut by a granitic dyke (Figure 10a), but it is not clear whether the dyke crosscuts the fault plane or not. In the foot wall close to the thrust, the damage zone contains NW-dipping shear bands with a top-to-the-SE sense of shear, consistent with the kinematics of the fault plane (Figures 4a, 4b, and 10d). A few meters from the Uganik Thrust in the Kodiak Landward Belt footwall, schists display a very dense network of quartz veins. The density of shear bands and veins decreases with increasing distance from the fault.

### 4.2. RSCM Temperatures

Temperatures obtained by RSCM are reported in Table S2, and average values of each analyzed sample are plotted in Figures 3–6. Representative Raman spectra of each formation/belt are plotted in Figure 11.

#### 4.2.1. Accreted Units

The average temperature for samples from the Uyak Complex in Uyak Bay is 256°C, in a range from 239 to 281°C (Figures 3 and 12; sites 19KO16, 19KO17F, 19KO18, 19KO19, 19KO20, 19KO21, and 19KO23). The Kodiak Landward Belt in Uyak Bay shows similar temperatures to the Uyak Complex ranging from 240 to 267°C (Figure 3), whereas further south in Uyak Bay, the Kodiak Formation is characterized by a discontinuous increase of temperature up to 382°C (Samples 22KO01-22KO28; Figure 3). At Big Waterfall Bay, where the

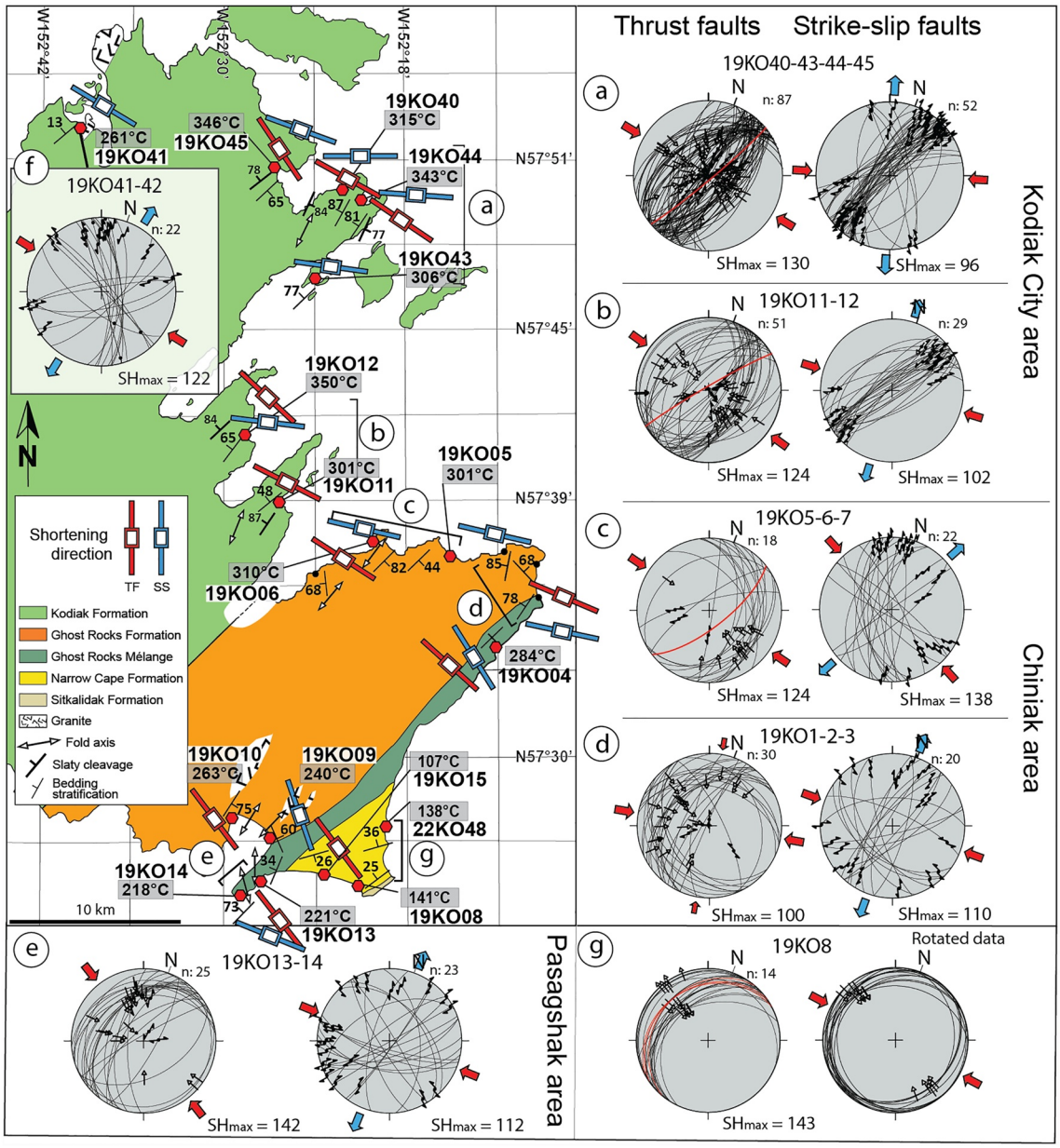


**Figure 5.** Geological map of the Kodiak Seaward Belt in the Kodiak City area, the Ghost Rocks Formation and the Narrow Cape Formation, showing measured stratification bedding and slaty cleavage (equal area, lower hemisphere stereonets) and Raman spectroscopy of carbonaceous material temperatures. Structural analysis indicates two deformational styles across both formations: earlier, conjugate thrust faults with a SE-NW shortening direction and later strike-slip faulting in the same shortening direction. (a) and (b) represent structural data for the Kodiak Seaward Belt, (c) and (d) for the Ghost Rocks Formation in the Chiniak area, and (e) for the Ghost Rocks Mélange in the Pasagshak area. (f) Stereonets of strike-slip faults in both the Kodiak granite and the surrounding schists. Red lines represent the average slaty cleavage for each area. (g) Orientation of normal and thrust faults in the Narrow Cape Formation on the left stereonet. When bedding is rotated back to horizontal, all faults become conjugate thrust faults as on the right stereonet.

Uganik Thrust is exposed, temperatures of the Uyak Complex in the hanging wall range between 262 and 299°C (sites 19KO25 and 19KO27), and the Kodiak Formation in the footwall shows a temperature range of 275–296°C (Figure 4; sites 19KO27 and 19KO28). The average values for both the foot wall and hanging wall are identical (282°C). The Kodiak Central Belt in Seal Bay is characterized by temperatures of 320–340°C (Figure 3; sites 19KO29-19KO39). For the Kodiak Seaward Belt in the Kodiak City area, temperatures average 325°C (305–348°C; Figure 5; sites 19KO11, 19KO12, 19KO40-19KO45). The lowest temperature among all samples from the Seaward Belt in the Kodiak City area is obtained in the schist from Anton Larsen Bay (261 ± 17°C; Site 19KO41), where the granitic intrusion is exposed. In the Old Harbor area, a wide range of temperatures is found

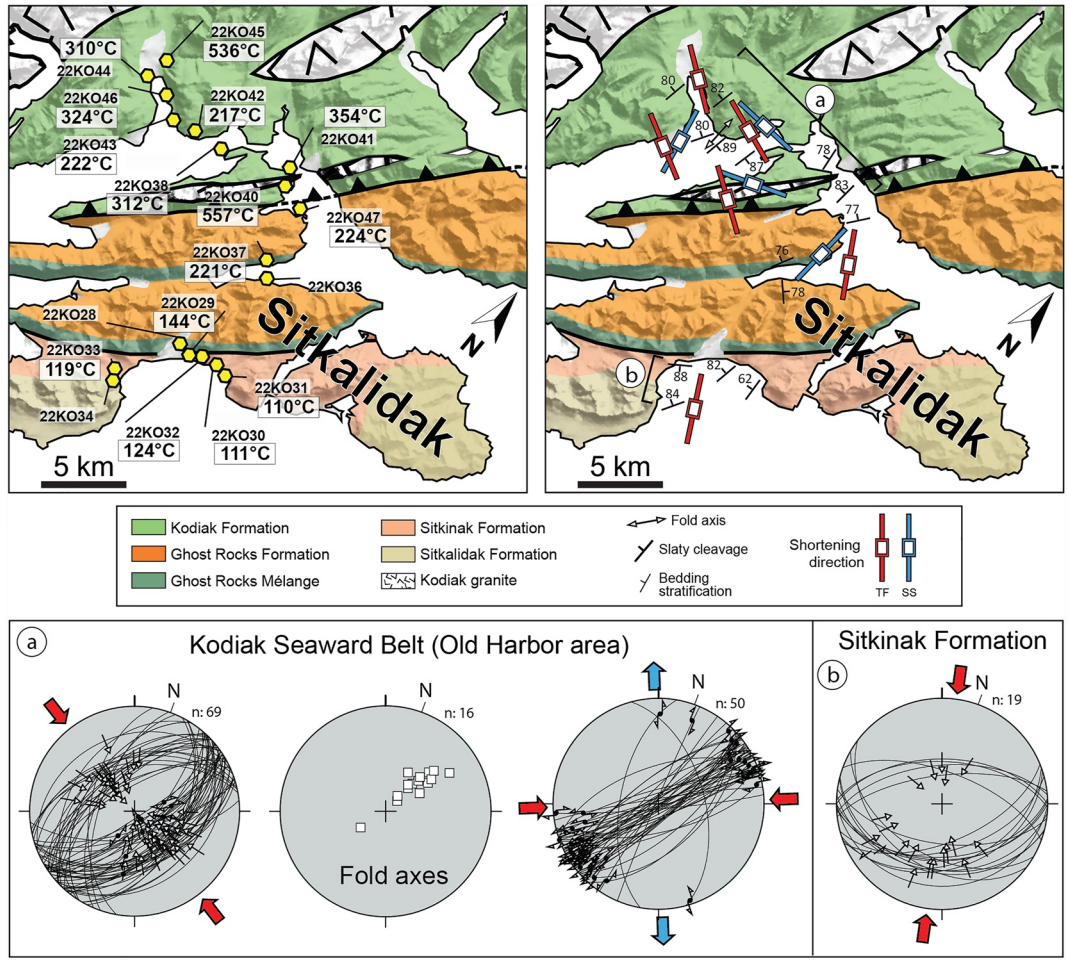


**Figure 6.** Geological map of the Old Harbor area with Raman spectroscopy of carbonaceous material temperature results and measured bedding and shortening directions derived from thrust and strike-slip faults. (a) Stereo diagram of main deformation structures in the Kodiak Seaward Belt (equal area, lower hemisphere): (left) Conjugate thrust faults, (center) isoclinal folds, and (right) strike-slip faults. (b) Thrust faults in the Sitkinak Formation at Sitkalidak Island.

(Figure 6). Four samples (22KO38, 22KO41, 22KO44, and 22KO46) yield temperatures in the range 310–354°C, while two samples show significantly lower temperatures of 217 ± 14°C (22KO42) and 222 ± 8°C (22KO43). The sample in the hanging wall of the Contact Fault (22KO40) near the granite intrusion yielded a temperature of 557 ± 16°C, similar to the sample 22KO45 (536 ± 18°C). In the Ghost Rocks Formation, the Chiniak area (Figure 5) is characterized by an average temperature of 295°C (279–309°C; sites 19KO4-19KO6), whereas the Pasagshak area yielded an average temperature of 227°C (218–241°C; sites 19KO9, 19KO10, 19KO13 and 19KO14). At Sitkalidak Island (Figure 6), two analyzed samples show equal temperatures of 224 ± 10°C (22KO47) and 221 ± 12°C (22KO37).

### 4.2.2. Slope Sediments

Samples from the Sitkinak and Narrow Cape Formations experienced peak-metamorphic temperatures below the limit of the method of Lahfid et al. (2010). Consequently, they were treated using the Schito et al. (2017) method.

Five samples from the Sitkinak Formation revealed similar temperature results to the Narrow Cape Formation. For sample 22KO29, an RA2 value of 1.06 ± 0.14 corresponds to Ro% of 1.39 ± 0.29, with a final temperature of 144 ± 7°C. Samples 22KO30 and 22KO31 have RA2 values of 0.78 ± 0.07 and 0.77 ± 0.07, corresponding to Ro% of 0.80 ± 0.15 and 0.78 ± 0.15, and yielding temperatures of 111 ± 14°C and 110 ± 14°C, respectively. Samples 22KO32 and 22KO33 have RA2 values of 0.87 ± 0.15 and 0.82 ± 0.09, giving Ro% values of 0.99 ± 0.3 and 0.89 ± 0.19, or temperatures of 124 ± 19°C and 119 ± 17°C, respectively (Figure 6).

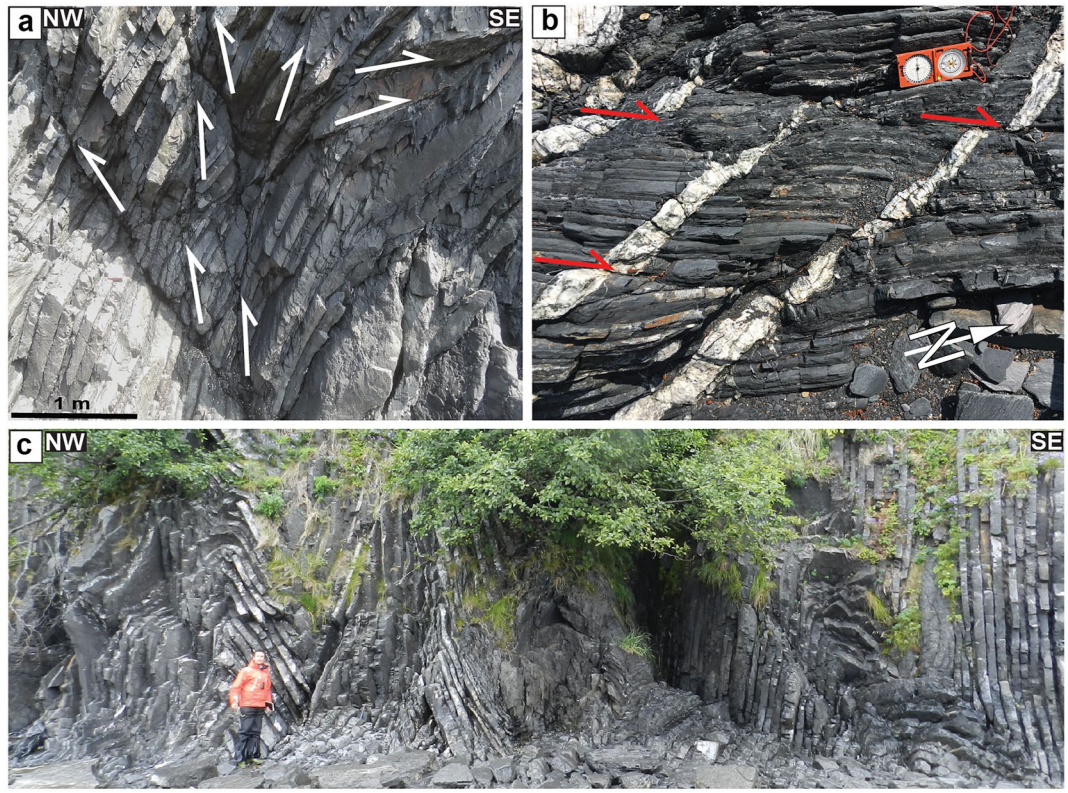


**Figure 7.** Preserved deformation structures in the Kodiak Seaward Belt: (a) Conjugate set of thrust faults indicating NW-SE shortening direction (Site 19KO44). (b) Late-stage dextral strike-slip faults offsetting subvertical quartz-calcite-chlorite veins (Site 19KO12). (c) Isoclinal folds in the Kodiak Seaward Belt, Old Harbor area (Site 22KO42).

For three samples of the Narrow Cape Formation, the average RA2 values are 0.72 ± 0.06 (19KO08), 0.82 ± 0.08 (19KO15), and 0.98 ± 0.14 (22KO48), with the majority of points ranging from 0.77 to 0.91. Estimated RA2 values are correlated to Ro (%) of 0.63–1.21 (0.92 ± 0.29; Schito et al., 2017), corresponding to the temperatures of 100 ± 13°C (19KO08), 119 ± 14°C (19KO15) and 138 ± 19°C (19KO15; Figure 5). Temperature results are in a narrow range for each sample (for 13–18 measurements in individual samples), within the limits of standard deviations proposed for the RSCM method (Beyssac et al., 2002; Lahfid et al., 2010; Schito et al., 2017).

## 5. Discussion

### 5.1. Deformation Kinematics Across the Complex

Our structural analysis points to a variable strain regime, particularly with respect to pure or simple shear. This variable strain regime persists despite the constant NW-SE direction of deformation across strike in the whole accretionary complex, similar to the present-day convergence direction of the Alaskan margin.

As previously proposed by Byrne (1982) and Connelly (1978), tectonic mélanges in Kodiak are characterized by top-to-the-SE (trench) simple shear deformation. This deformation is also present in the Kodiak Landward Belt, near the Uganik Thrust (D. M. Fisher & Byrne, 1987; Sample & Fisher, 1986). In contrast, the coherent units that constitute the frontal part of the prism (the Kodiak Seaward Belt and Ghost Rocks Formation) are characterized by horizontal shortening evidenced by sub-vertical slaty cleavage, conjugate thrust faults and folds with sub-vertical axial planes (Figures 5 and 6; Byrne, 1982). While Sample & Moore (1987) described only top-to-the-SE thrust faults in those two formations, we observed an equal amount of top-to-the-NW thrust faults that points to strong NW-SE horizontal shortening (Figures 5a, 5b, and 6a). Furthermore, the orientation of isoclinal folds is compatible with such shortening (Figure 6a). The lack of thrust faults in the Kodiak granite indicates that the horizontal shortening predates intrusion emplacement, which is also supported by xenoliths containing cleaved rocks in different orientations.

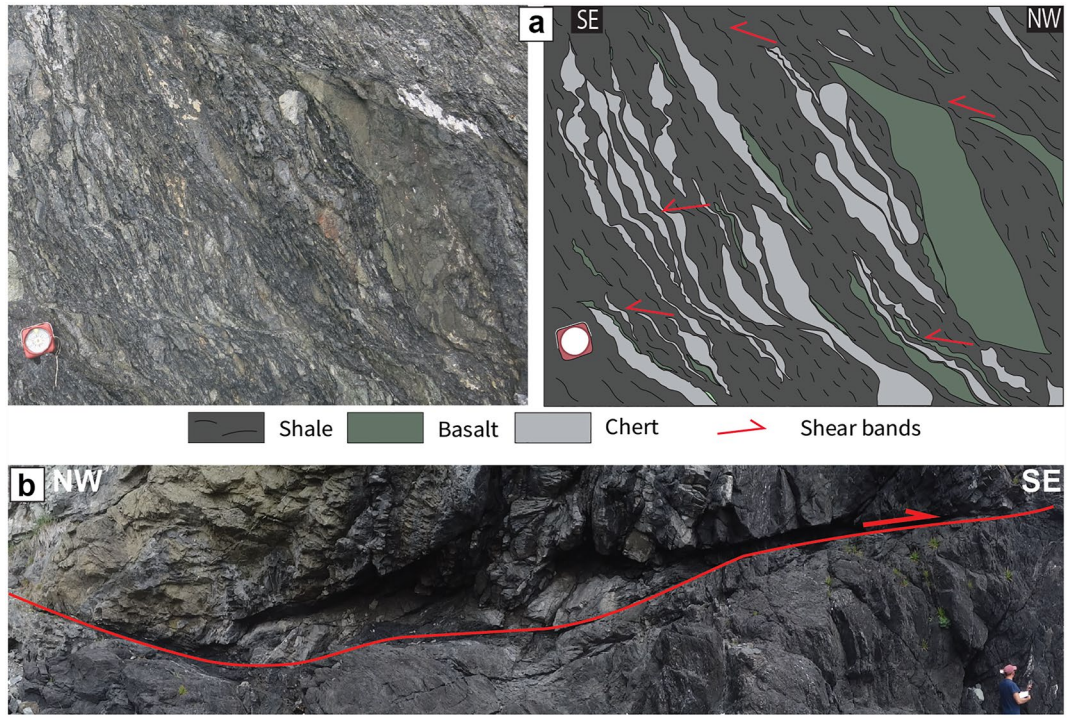


**Figure 8.** Representative deformation structures in the tectonic mélanges of the Kodiak accretionary complex. (a) Non-coaxial deformation evidenced by top-to-the-SE shear bands, Uyak Complex (Site 19KO17F). (b) Large-scale top-to-the-SE thrust fault in the Ghost Rocks Mélange, Pasagshak area (Site 19KO14).

The only exception to this shortening deformation in coherent units is found in a few outcrops in the Kodiak Central Belt, where we observed extensional shear bands (Figures 2b and 4c). The kinematics and timing of deformation in the Kodiak Central Belt are nevertheless disputed. Sample & Moore (1987) also reported normal faults often in conjugate sets, but they proposed that such normal faults formed after the intrusive event. However, normal shear bands found during this study contain textural evidence suggesting that they formed at peak metamorphic conditions, further supported by multi-phase equilibrium model from illite and chlorite in contact with such bands (Rajič, Raimbourg, Lerouge, et al., 2023). Quartz-filled extensional shear bands are already reported (D. M. Fisher & Byrne, 1987, 1990; D. M. Fisher et al., 1995). However, these shear bands are not described as conjugate sets but as dominated by top-to-the-SE shear deformation, also visible in an abundant en-échelon array of quartz veins. Further work is therefore needed to clarify the deformation kinematics in the Central Belt.

Closer to the trench, slope sediments record horizontal shortening with variable intensity between formations. The Sitkinak Formation experienced significant horizontal shortening and tilting of strata to vertical position (Figure 6b). The Narrow Cape Formation, on the contrary, experienced less deformation. Still, a contractional regime is documented (Figure 5g). Thus, both formations record a period of horizontal shortening post-dating the Oligocene and possibly even the Miocene.

Overall, our structural data imply that at least two periods of horizontal shortening affected the Kodiak accretionary complex. The first is recorded in basally accreted units and occurred before the intrusive event, and the second occurred after the sedimentation of slope sediments.

### 5.2. Temperature Structure of the Complex

#### 5.2.1. Large-Scale Antiformal Structure

Temperatures results from this study indicate that relatively high temperatures (300–380°C) are recorded in the central part of the complex, the Kodiak Central and Seaward Belts, and decrease (220–300°C) toward the inner and outer domains (Landward Belt and Uyak Complex, and Ghost Rocks Formation, respectively, Figure 12).

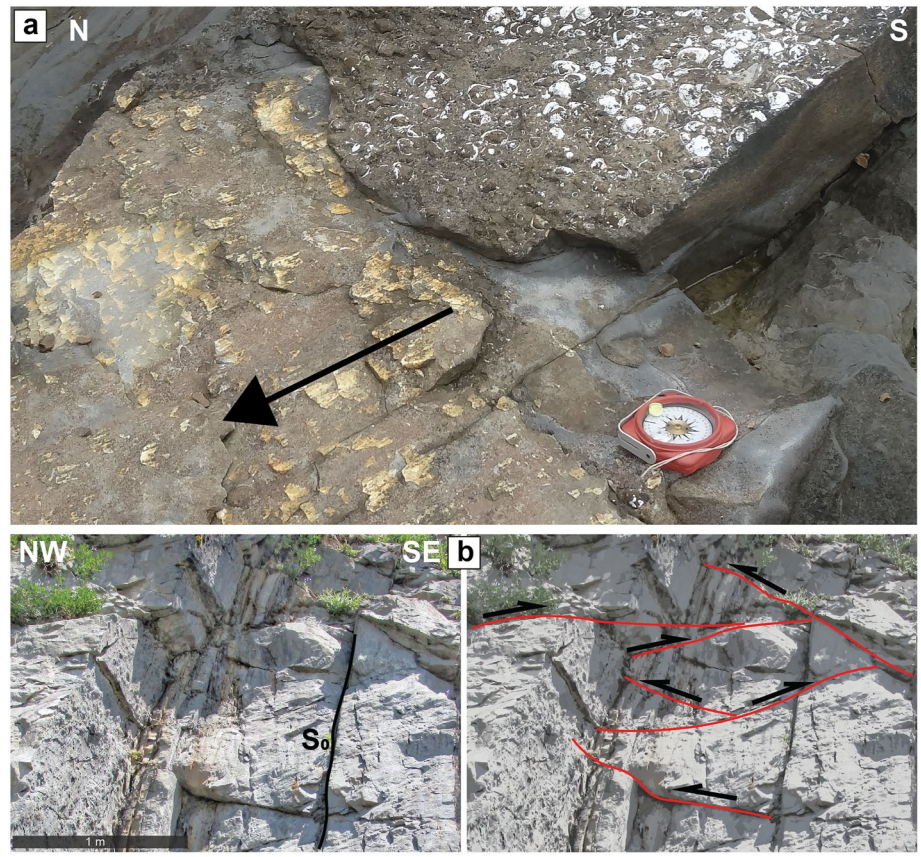


**Figure 9.** Representative deformation structures in slope sediment units of the Kodiak accretionary complex. (a) An example of a low-angle normal fault in the Narrow Cape Formation (Site 19KO08). (b) Sub-vertical bedding stratification and conjugate thrust faults in the Sitkinak Formation (Site 22KO29).

This finding is at odds with previous studies where a monotonous trenchward decrease is expected along the studied profile (Brantley & Fisher, 1997; Moore et al., 1983; Roeske et al., 1989; Rowe et al., 2009; Vrolijk et al., 1988). The only zone which potentially indicates trenchward cooling is observed in the Ghost Rocks Formation (Figure 12).

Based on the orientation of the bedding stratification (sub-vertical in the Landward and Seaward Belts and sub-horizontal in the Central Belt), D. M. Fisher and Byrne (1992) proposed an antiformal structure within the Kodiak Formation, where the Central Belt represents its core and the Landward and Seaward Belts its limbs. Our temperature profile, where samples are plotted relative to the orthogonal distance to the Contact Fault, is in agreement with large-scale fold geometry, assuming that the temperatures were acquired during deformation, and passively transported during folding (Figure 12). The orientation of the crenulation cleavage throughout the Kodiak and Ghost Rocks Formations suggests that the antiform is asymmetrical and inclined toward the trench. The large wavelength of such folding (>50 km) at the scale of the whole belt does not significantly rotate the preexisting upright folds of the Kodiak Seaward Belt and the Ghost Rocks Formation. The antiform likely formed during a period of horizontal shortening, which is most pervasive in the frontal part of the complex.

The thermal structure of the Kodiak complex can be compared to several well-studied accretionary prisms across the globe. In the Franciscan complex (California) or the Shimanto and Sambagawa belts (southwestern Japan), for instance, metasedimentary units record a continuous increase in *P-T* conditions from the paleo-trench position to the inner domains (Ernst & McLaughlin, 2012; Osozawa & Wakabayashi, 2015; Palazzin et al., 2016; Raimbourg et al., 2014; Tagami & Dumitru, 1996; Wakabayashi, 2015). Contrary to the Franciscan complex and southwestern Japan, the Otago Schists in New Zealand show an antiform structure, from pumpellyite-prehnite facies in outer parts of the antiform to garnet-biotite-albite zone in its core (Breeding & Ague, 2002; Mortimer, 2000). Forster and Lister (2003) suggested that the higher-grade metamorphic core of this antiform is exhumed due

10.1029/2023TC007754

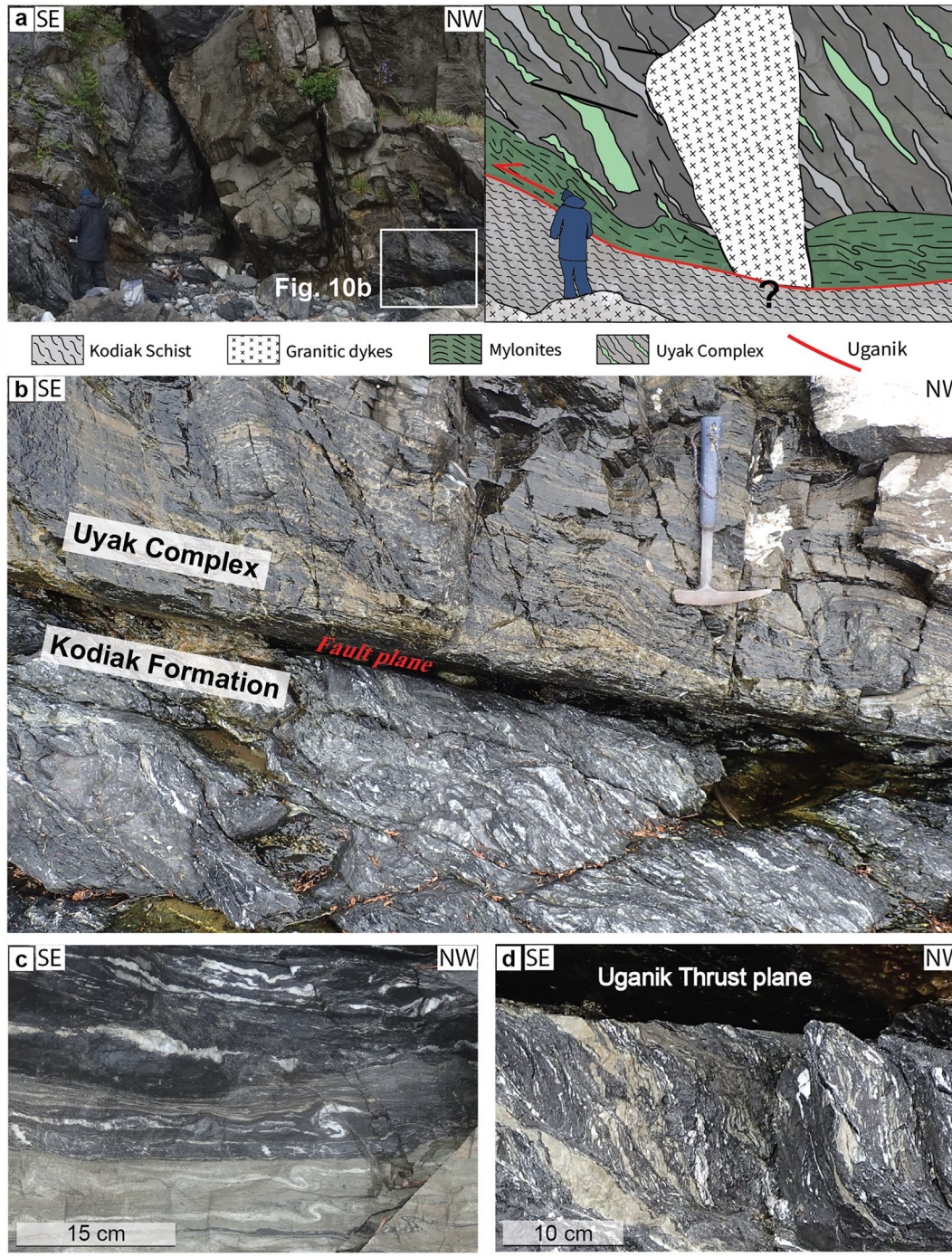


**Figure 10.** (a) The Uganik Thrust at Big Waterfall Bay. (b) Uganik Fault plane with a mylonitic hanging wall (Uyak Complex) and highly sheared sediments in the foot wall (Kodiak Formation). (c) Asymmetric folds in the mylonite indicate a top-to-the-SE sense of shear. (d) Highly sheared sediments in the foot wall.

to extensional tectonics and erosion. The distribution of our thermal data shown in Figure 12 indicates that the Kodiak accretionary complex is more similar to the Otago Schist, with temperature variations indicating structural relief associated with a post-accretion anticlinorium. However, extensional tectonics, as proposed in the Otago Schist, are not observed within the Kodiak complex and cannot be responsible for the exhumation of the whole structure.

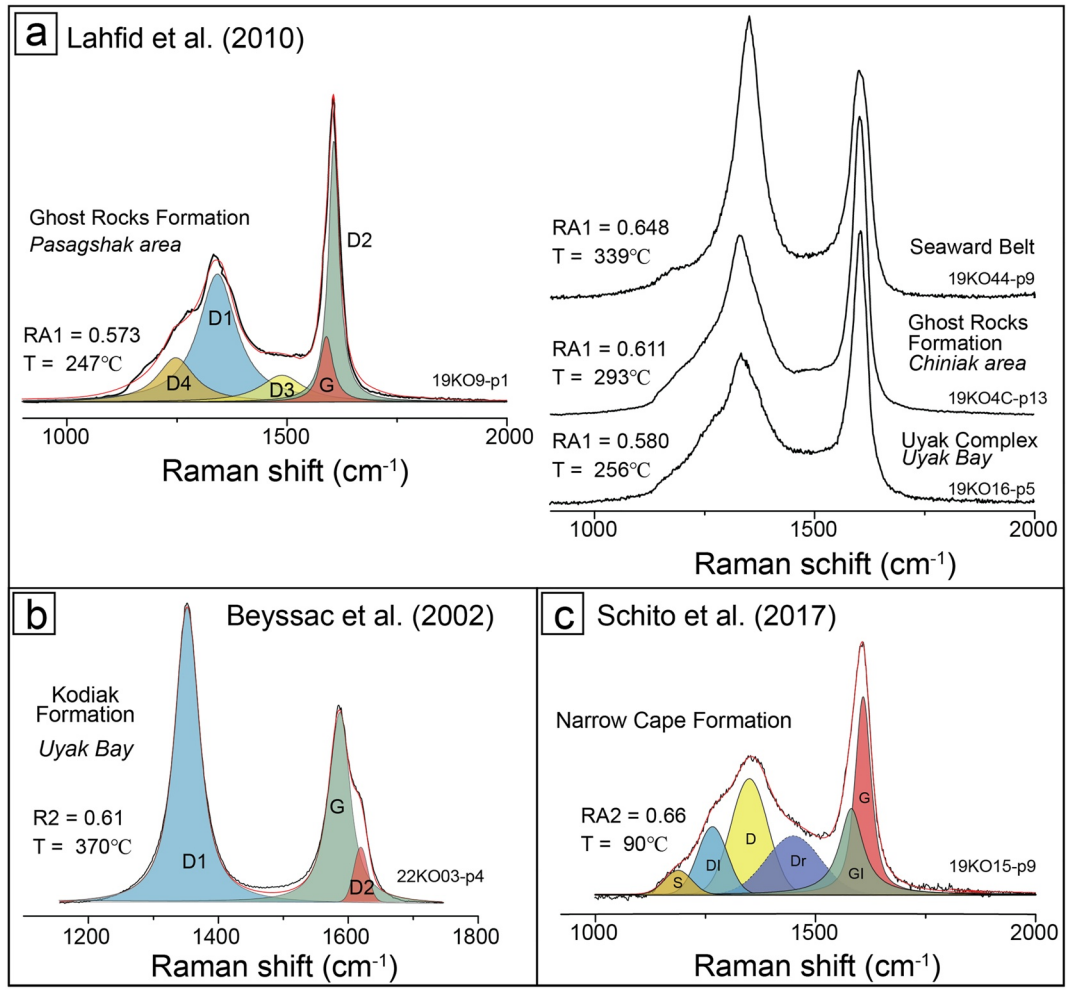


**Figure 11.** (a) Representative Raman spectra for each accreted formation/belt deconvoluted according to the method of (a) Lahfid et al. (2010), (b) Beyssac et al. (2002), and (c) Schito et al. (2017).

### 5.2.2. Influence of Plutonism on Raman T Profile

As the Kodiak accretionary complex experienced pervasive plutonism during ridge subduction (Farris, 2010; Farris & Haeussler, 2020; Farris et al., 2006), one can ask whether carbonaceous material was affected by contact metamorphism during plutonism. Several studies concerning the degree of recrystallization of carbonaceous material during contact metamorphism pointed out that temperatures derived by RSCM are in agreement with the estimates derived by mineral phase equilibrium (e.g., Aoya et al., 2010; Beyssac et al., 2019; Delchini et al., 2016; Hilchie & Jamieson, 2014). Moreover, in some cases, such as the Halifax, Nova Scotia (Hilchie & Jamieson, 2014) or the Jebilet massif, Morocco (Delchini et al., 2016), greenschist facies rocks outside the contact aureole that contain no evidence of mineralogical changes due to the contact metamorphism are characterized as well by the lowest temperature estimates by RSCM. This suggests that the influence of contact metamorphism on a degree of recrystallization of carbonaceous material can be traced simply by following mineralogical changes caused by contact metamorphism.

In the Kodiak complex, the Kodiak Batholith has been the subject of several studies (Farris, 2010; Farris & Haeussler, 2020; Farris & Paterson, 2009; Farris et al., 2006). First, Farris et al. (2006) estimated the biotite isograds to have reached a width up to 5 km away from the Kodiak Batholith and ~0.15 times the radii of smaller plutons. This means that, in parallel to the studies mentioned above (e.g., Delchini et al., 2016; Hilchie & Jamieson, 2014), the influence of the contact metamorphism onto carbonaceous material is probably restricted to the cordierite and biotite zones, no more than 5 km away from the Kodiak Batholith at a maximum (Farris et al., 2006), while the decrease in temperature observed in RSCM temperature is almost continuous from the

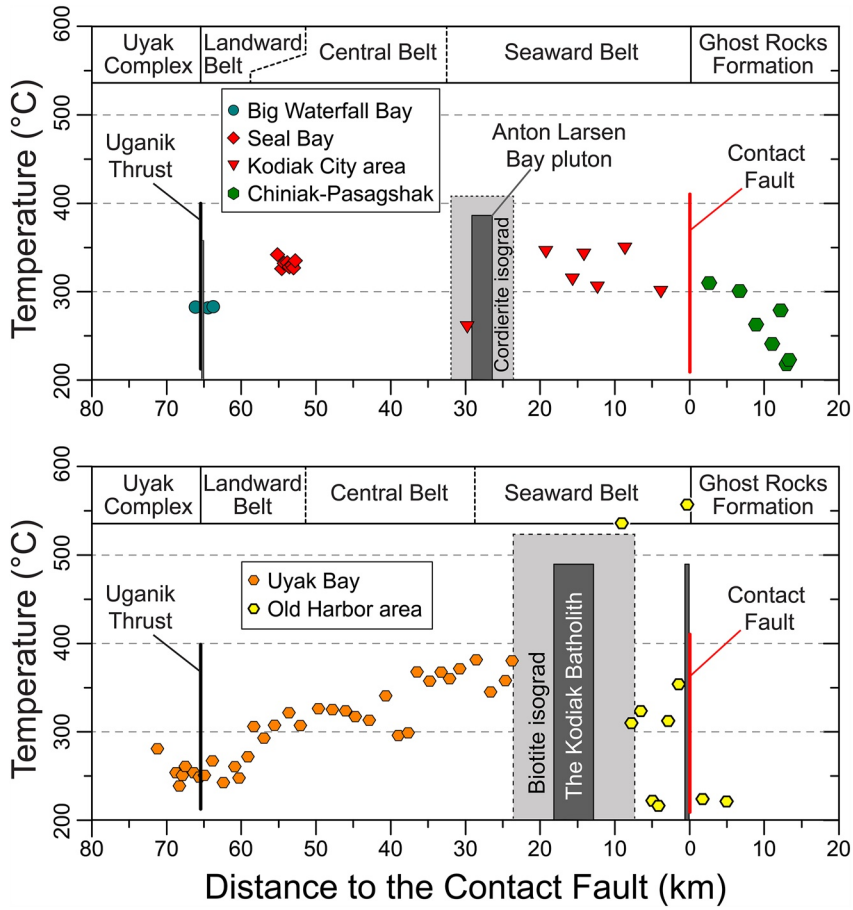


**Figure 12.** Raman spectroscopy of carbonaceous material temperature profiles from all accreted units examined in this study, the Anton Larsen pluton, and the Kodiak Batholith with associated cordierite/biotite isograds (Farris et al., 2006). For the Kodiak City area, Old Harbor area, and Uyak Bay, results are plotted with respect to the distance to the Contact Fault, whereas results from Big Waterfall Bay and Seal Bay are plotted with respect to the distance to the Uganik Thrust.

Kodiak Batholith for over 30 km (Figure 12). There is no "hidden" magmatic body, as gravity transects indicate that the batholiths exhibits steeply-dipping boundaries (Farris et al., 2006), meaning that the thermal influence onto metasediments is the same at all levels of exposure. Accordingly, only two samples located in the cordierite and biotite zones of the contact metamorphism (22KO40 and 22KO45) exhibit high temperatures over 500°C (Figure 6; Table S2) that may reflect the influence of the pluton on the RSCM temperature record. Finally, the asymmetric shape of the temperature profile of Uyak Bay disagrees with a possible thermal imprint of the Kodiak Batholith (Figure 12).

Furthermore, the cross-cutting relationships between plutons and metamorphic cleavage show magma emplacement postdated deformation (Byrne & Fisher, 1987; Sample & Fisher, 1986; Sample & Moore, 1987). In these cleavage structures, the metamorphic temperature conditions inferred by the multi-phase equilibrium model from cleavage-forming minerals closely match those implied by RSCM (Rajič, Raimbourg, Lerouge, et al., 2023). Also, metamorphic illite and chlorite used to decipher pressure-temperature conditions are characterized by significantly larger grain sizes in contact with shear bands, meaning that they crystallized contemporaneously with the main deformation event (Rajič, Raimbourg, Lerouge, et al., 2023). This suggests that the RSCM temperatures are syn-tectonic and predate magmatism, ruling out the possibility that the latter is the primary control on the RSCM temperature field. In addition, chlorite thermometry revealed similar results as in the Valdez Group, an equivalent of the Kodiak Formation to the northeast on the mainland (Weinberger & Sisson, 2003), in which the magmatic intrusions are less abundant.

In summary, all the arguments listed above suggest that the estimated temperatures by RSCM represent syn-subduction temperatures with a later thermal influence from magmatic bodies restricted to those

metasediments (such as in samples 22KO40 and 22KO45) that are located near the intrusions (Figures 6 and 12). Thus, the thermal profile observed in this study is likely a result of horizontal shortening within the wedge, as discussed above, with only a local influence by contact metamorphism.

#### 5.2.3. Ridge Subduction and Geothermal Gradient

During ridge subduction, the thermal structure of a subduction zone is profoundly changed, and anomalously high geothermal gradients can be reached (Bradley et al., 2003; DeLong et al., 1979). In the case of the Kodiak complex, several attempts have been made to estimate the prism geothermal gradient (Moore et al., 1983; Myers & Vrolijk, 1986; Rajič, Raimbourg, Lerouge, et al., 2023). Based on a multi-phase equilibrium model, estimated pressure-temperature conditions for the Kodiak Central Belt suggest that the geothermal gradient was ∼30°C/km (Rajič, Raimbourg, Lerouge, et al., 2023), similar to the estimations derived from fluid inclusions for the Kodiak and Ghost Rocks Formations (Vrolijk et al., 1988). As the Kodiak and Ghost Rocks Formations have been accreted prior to ridge subduction (Byrne & Fisher, 1987; Farris & Paterson, 2009; Farris et al., 2006; Moore et al., 1983; Sample & Moore, 1987), it is expected that very young and hot oceanic crust subducted and consequently affected the thermal structure of a subduction zone.

A similar model has been proposed for the Shimanto Belt between the Cretaceous and Eocene, where the estimated geothermal gradient of ∼20°C/km (Raimbourg et al., 2014; Rajič, Raimbourg, Lerouge, et al., 2023; Toriumi & Teruya, 1988) was attributed to the subduction of very young and hot oceanic crust prior to ridge subduction (Sakaguchi, 1999).

### 5.3. Temperature Structure Around the Uganik Thrust

The Uganik Thrust, interpreted as an out-of-sequence thrust (Rowe et al., 2009), is the only exposed large-scale fault zone on the northwestern side of the accretionary prism. The deformation zone comprises a sharp fault plane. Damage zones on both sides of the fault are characterized by a high density of top-to-the-trench shear bands (Figure 10). In the Kodiak Landward Belt, top-to-the-trench simple shear only occurs close to the Uganik Thrust (Figure 3). The kinematics of the Uganik Thrust plane itself and the shear bands in the Kodiak Landward Belt are very similar (Figures 4a and 4b): several south-verging shear zones with N-S trending slickenlines have been measured in the Kodiak Landward Belt, almost parallel to the slip direction of the Uganik Thrust fault (Rowe et al., 2009). Most deformation predates magmatism, as dykes cut across the shear zones of the footwall and the hanging wall. We could not decipher the relationship between the Uganik Thrust sharp fault plane and the magmatic intrusions, whereas Rowe et al. (2009) interpreted the last motion on the main fault plane and the magmatic event as contemporaneous.

At the two exposures of the Uganik Thrust located in Uyak and Big Waterfall Bays, our RSCM paleothermometry results point to a lack of a thermal gap across the hanging wall and footwall of the fault. In Uyak Bay, the temperature gap of ∼10°C in the vicinity of the thrust is well below the uncertainty of temperature estimates by RSCM (∼30°C, Lahfid et al., 2010). The average temperatures from the Landward Belt and the Uyak Complex are also indistinguishable (Figure 12). This relationship is also found in Big Waterfall Bay, where both sides of the thrust recorded a temperature of ∼285°C. Also, the RSCM temperature range for the Landward Belt in Big Waterfall Bay is very close to the temperature results inferred from vitrinite reflectance (Rowe et al., 2009).

A thermal gap across out-of-sequence thrusts is reported in several accretionary complexes caused by the juxtaposition of rocks buried at different depths (e.g., Nobeoka Tectonic Line in the Shimanto Belt; D. M. Fisher et al., 2019; Kondo et al., 2005; Raimbourg et al., 2017). For the Uganik Thrust, Rowe et al. (2009) proposed that the thermal gap of 0–45°C existed between the foot wall and hanging wall but was later overprinted by a thermal peak caused by ridge subduction and focused flow of hot fluids along the faults. Such interpretation is ruled out by the thermal profiles (Figure 12), where no thermal anomaly on the thrust itself and its immediate vicinity has been observed.

A broader question arises as to whether the RSCM temperatures reflect syn-tectonic conditions or a post-tectonic thermal overprint related to magmatism. We favor first interpretation due to the following reasons. The magmatic intrusions are of relatively small size with respect to the whole volume of the investigated areas. In particular, in Big Waterfall Bay, the observable magmatism is restricted to meter-scale dykes unlikely to affect the map-scale temperature field. The main dyke near the Uganik Thrust has a thickness of ∼15 m (Rowe et al., 2009). It is

unlikely that such dyke would thermally influence a larger area, such as 1 km from the Uganik Thrust (Sample 19KO28), where the temperature results are identical or even slightly higher than that of the metasediments a few meters away from the thrust and the dyke (Figure 4). The thermal influence of a magmatic dyke over sedimentary host rock has been studied in the Kinsho-zan area, Japan, where a 13 m thick andesitic dyke intruded the Akasaka Limestone (Mori et al., 2015). Their results show that the limestone is thermally affected only in the domain within 3 m from the dyke, with a significantly smaller thermal influence than the prediction of thermal models (Mori et al., 2015). Thus, the limited possible thermal influence of dykes and the absence of any observed thermal gap across the Uganik Thrust in Uyak Bay (Figure 3) and Big Waterfall Bay (Figure 4) leads to the conclusion that the estimated temperatures represent syn-subduction conditions.

Consequently, the lack of a thermal gap between the foot wall and hanging wall of the Uganik Thrust suggests that most of the slip occurred while the fault was a plate boundary décollement. Thus, combining deformation structures with temperature results, we propose that the Uganik Thrust first acted as a plate-boundary interface during underthrusting and accretion of the Kodiak Formation rather than as an out-of-sequence thrust as proposed by Rowe et al. (2009) and then later reactivated as the south-verging thrust fault without significant offset.

### 5.4. Vertical Motion in the Frontal Part of the Complex

Combining our results with results from previous studies, three different stages of vertical motion in the Kodiak accretionary complex are recognized (Figure 14). The approximate amplitudes of exhumation/rock subsidence are estimated assuming a geotherm of 30°C/km inferred from multi-phase equilibrium in the Kodiak Formation (Rajič, Raimbourg, Lerouge, et al., 2023) and based on vitrinite reflectance and porosity data in the Sitkalidak and Sitkinak Formations (Moore & Allwardt, 1980). The duration of each period is calculated based on the available geochronological constraints (Byrne, 1982; Byrne & Fisher, 1987; Moore & Allwardt, 1980; Moore et al., 1983).

The cooling and exhumation of the Late Cretaceous-Early Paleogene units are proposed to occur due to basal accretion of the Eocene sediments (Byrne, 1986; Byrne & Fisher, 1987). In parallel, zircon and apatite fission-tracks studies suggest that cooling of the Late Cretaceous-Early Paleogene units occurred during the Eocene, around 50–55 Ma (Clendenen et al., 2003). However, the authors pointed out that such cooling ages coincide with the intrusive event related to ridge subduction, potentially indicating a reset of zircon fission track ages in the Kodiak Central Belt (Clendenen et al., 2003). In any case, the exhumation is likely promoted by prism thickening in combination with surficial erosion since normal faulting is scarcely observed throughout the complex. The lack of thermal gaps across the complex, in first-order along the large-scale faults, points to the exhumation of all units as a single body.

To exhume the deeply buried units, the Uyak Complex, and the Kodiak and Ghost Rocks Formations, 7–13 km of material must have been removed from the top of the wedge by erosion (combining the peak temperatures with the geothermal gradient of 30°C/km). Although the exact time of initiation of exhumation is challenging to define, we estimate the duration of exhumation to have occurred over 22–39 My; we assume the beginning of exhumation between 65 and 50 Ma, given the depositional age of the Kodiak and Ghost Rocks Formations is 73–60 Ma (Byrne & Fisher, 1987), or as estimated by the zircon and apatite fission-tracks studies (Clendenen et al., 2003). The end of the exhumation event is assumed as the first depositional age of slope sediments, around 26 to 28 Ma (Moore & Allwardt, 1980). Thus, the estimated exhumation rate of the Kodiak and Ghost Rocks Formations through the (Paleocene)-Eocene is 0.18–0.6 mm/yr (for an amplitude of 7–13 km). These exhumation rates are similar to rates derived from zircon and apatite fission track analyses in the Valdez Group (∼0.5 mm/yr; Arkle et al., 2013), an equivalent to the Kodiak Formation at Kenai Peninsula to the northeast.

The surficial erosion from the top (7–13 km, depending on the peak temperatures) implies a flux of sediment toward the trench during the Eocene-Oligocene. Combining peak temperatures in each formation/belt with the geothermal gradient of 30°C/km and the approximate length of the complex (∼120 km), our calculations point to a sediment supply to the trench ranging from 36 to 62 $km^2$ $m.y.^{-1}$. This range is comparable with the sediment supply in ancient and recent accretive margins, such as the SE Alaskan margin in the Eocene-Oligocene (50–100 $km^2$ $m.y.^{-1}$; Moore et al., 1991), or recent examples such as the Aleutian margin and the Nankai Trough (54 and 65 $km^2$ $m.y.^{-1}$, respectively; Clift and Vannucchi (2004) and references therein).

After the end of exhumation of the Cretaceous-Paleogene accreted units, deposition of slope sediments onto the accreted units represents the beginning of the formation of accommodation space in the frontal part of the prism,

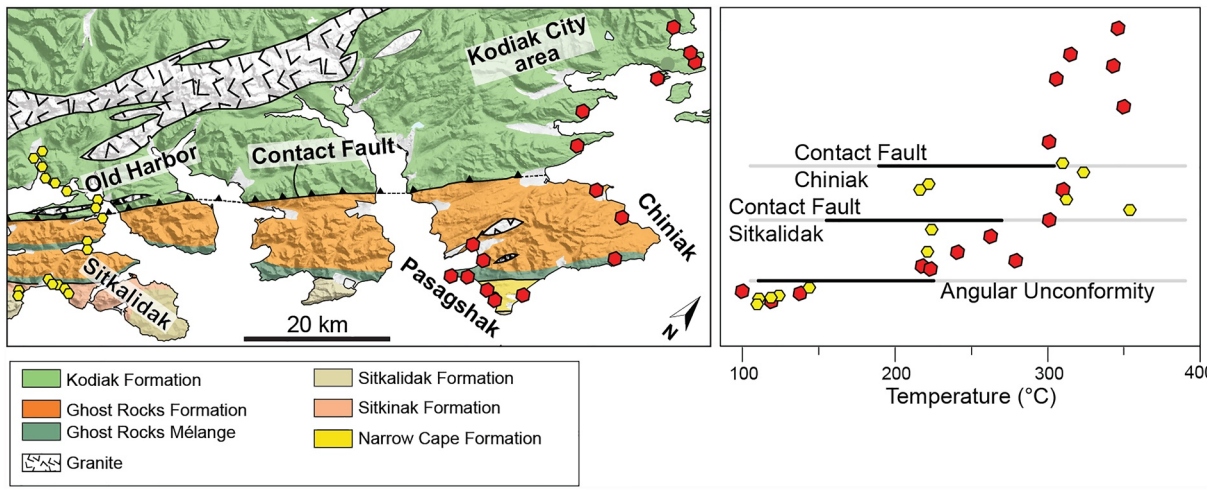


**Figure 13.** Raman spectroscopy of carbonaceous material temperature profile in the frontal part of the complex. Note the thermal gap of ~100°C between basally accreted Ghost Rocks Mélange and slope sediment formations, the Narrow Cape and Sitkinak Formations.

which the temperature data suggest is produced by subsidence (Figure 14). The temperature gap along the angular unconformity between the basally accreted units and the slope sediments is about 100°C (Figure 13). Slope sediments of the Sitkinak and Narrow Cape Formations are characterized by temperatures of 100–140°C, with most measurements clustering around 120°C. The temperatures of 120°C point to a large amount of rock subsidence and burial down to ~4 km, considering a thermal gradient of about 30°C/km (Moore & Allwardt, 1980). The oldest record of slope sedimentation is from the Oligocene Sitkinak Formation, the base of which is assumed to represent the onset of subsidence. The end of the subsidence at this position in the margin is difficult to estimate. However, a plausible possibility is during the Pliocene (3–6 Ma), which coincides with a rise in sedimentation rate in the trench compared to the Oligo-Miocene (Noda & Miyakawa, 2017; von Huene et al., 2012), and could cause the creation of relief on land. Hence, the duration of this local subsidence is estimated as 20–22 My, between the Oligocene and the Pliocene (3–6 Ma). Combined with the depths derived from the RSCM temperature results

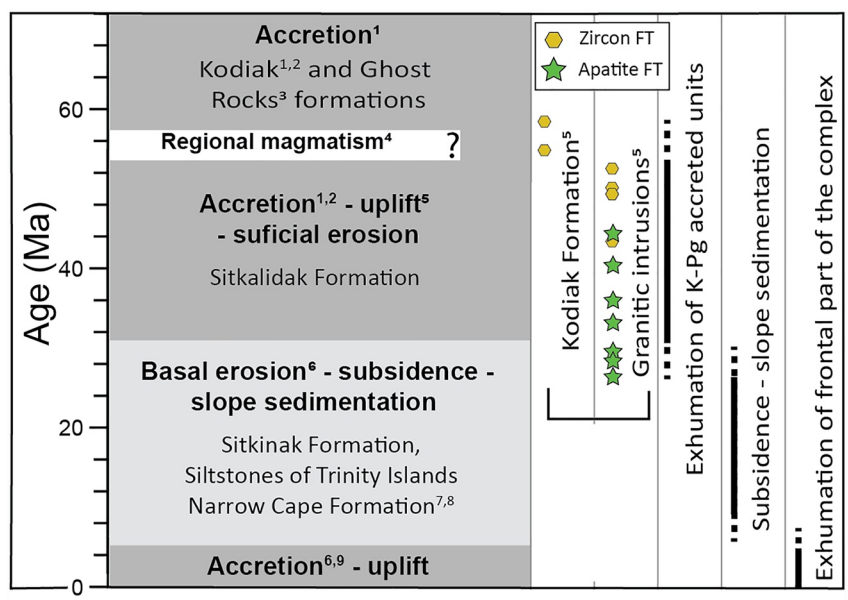


**Figure 14.** Summary of different periods of basal accretion and slope sedimentation combined with periods of exhumation and subsidence in the Kodiak accretionary complex. References: 1—(Byrne, 1986); 2—Byrne and Fisher (1987); 3—Byrne (1982); 4—Farris et al. (2006); 5—Clendenen et al. (2003); 6—von Huene et al. (2012); 7—Moore and Allwardt (1980); 8—Moore et al. (1983); 9—Noda and Miyakawa (2017).

(4 km), the calculated rock subsidence rate is 0.18–0.2 mm/yr. To explain such subsidence, four possibilities are discussed below: (a) Pervasive normal faulting, for example, due to prism instability following basal accretion (e.g., Corrado et al., 2019). (b) the presence of a slab tear beneath the accretionary wedge (Ascione et al., 2012; Ciarcia & Vitale, 2013). (c) Top-wedge basin formation related to the upper plate thrust fault systems. (d) A period of subduction erosion instead of accretion (Clift & Vannucchi, 2004).

First, according to our observations of deformation structures across the complex, normal faulting is too limited to contribute significantly to subsidence. Second, no slab tear is reported, as continuous subduction of the Pacific plate has occurred since at least 40 My (Müller et al., 2008). Third, from the analogy with modern offshore basins, local subsidence in top-wedge basins is another possibility to explain the vertical motions recorded in fossil rocks. In the slope southeast from the Kodiak archipelago, several basins have been formed, such as the Tugidak (M. A. Fisher, 1979, 1980) or Albatross basins (M. A. Hisher & Holmes, 1980; von Huene et al., 2012), pointing to local (and recent) subsidence. The processes that lead to such contemporary offshore basins forming are still ambiguous and potentially related to thrust fault systems and the consequent subsidence on both sides of the thrust systems (M. A. Fisher & Holmes, 1980; Morell et al., 2019; Noda & Miyakawa, 2017).

A good example is the Albatross Basin, located southeast of the Kodiak Island (M. A. Fisher & Holmes, 1980; von Huene et al., 2012). This basin is limited trenchward by the Albatross Bank fault system and landward by the Kodiak Shelf Fault System (Ramos et al., 2022). Such a thrust fault could produce subsidence and accommodate space either as a piggy-back basin or by subsidence in the footwall of active thrust faults. Finally, the deposition of the Sitkinak and Narrow Cape Formations coincides with the proposed period of subduction erosion during the Miocene by Von Huene et al. (2012) based on the fact that the current slope is made of Eocene or older rocks in contact with Quaternary sediments, suggesting that a large volume of material is basally eroded. This type of erosive subduction is also supported by Deep Sea Drilling Project Leg 18, Site 178 (Kulm et al., 1973), which found another unconformity between the Pliocene and Miocene slope sediments.

The final stage is the exhumation of previously buried units in the frontal part of the complex to their present position (Figure 14). The exhumation of the slope sediments buried down to ∼120°C requires surficial erosion of ∼4 km of material, yielding an estimated exhumation rate of about 0.8–1.3 mm/yr. After slope sedimentation, horizontal shortening occurred in those slope sediments, and strain is significant in the Sitkinak Formation, where the bedding stratification is vertically tilted. Thus, the exhumation can result from horizontal shortening in combination with surficial erosion. However, in the Narrow Cape Formation, shortening is not as pervasive as in the Sitkinak Formation, and an additional process is potentially required to exhume deeply buried sediments, such as uplift along the thrust such as the currently-active Kodiak Shelf Fault Zone (Carver et al., 2013; Ramos et al., 2022). Carver et al. (2013) pointed to a higher current uplift rate (∼0.75 mm/yr) in the Narrow Cape Formation than in the rest of the Kodiak Island, related to the active upper crustal faulting in the Kodiak shelf fault zone (Figure 15). These faults are steep and left-lateral in sense, with a significant up-to-the-NW vertical component (Carver et al., 2013). Also, since the Pliocene, a much larger sediment flux has been observed in trench sediments (Noda & Miyakawa, 2017; von Huene et al., 2012), which may lead to accelerated accretion and prism growth. Similar exhumation rates are reported in the very frontal section of the Prince William Sound, Southern Alaska (Arkle et al., 2013). Based on zircon and apatite fission track analyses, calculated rates are 1.0–2.4 mm/yr since the Pliocene (Arkle et al., 2013), related to a higher sediment input into the trench and, consequently, underplating of sediments.

Calculated exhumation and burial rates in this work (0.2–1.3 mm/yr) are comparable with previous estimations in exhumed paleo-accretionary wedges such as the Chugach Terrane (Arkle et al., 2013) or the Cascadia accretionary wedge at the Olympic Mountains, USA (Brandon et al., 1998), as well as with the exhumation of HP-LT of underplated duplexes (Agard et al., 2009; Guillot et al., 2009), or inferred from thermo-mechanical models (e.g., Angiboust et al., 2021; Menant et al., 2020). Also, our rates agree with tectonically-induced exhumation, estimated to occur at rates <4 mm/yr (e.g., Yamato et al., 2008). The burial depths (7–13 km for basally accreted units and 4 km for slope sediments) imply a large amplitude of burial/exhumation in the forearc. Similar vertical motions and temperature gaps at the unconformity between accreted and slope sediment units have been observed in the Shimanto Belt (Raimbourg et al., 2017), implying three stages of motion: (a) exhumation of the basally accreted units (buried at peak temperature of 300–350°C) to the surface due to collision and surficial erosion removal of about 3–8 km of material; (b) Subsidence and sedimentation of forearc Misaki Group on top of the previously exhumed units, and burial down to 170–250°C; (c) the exhumation of the Misaki Group to the surface.

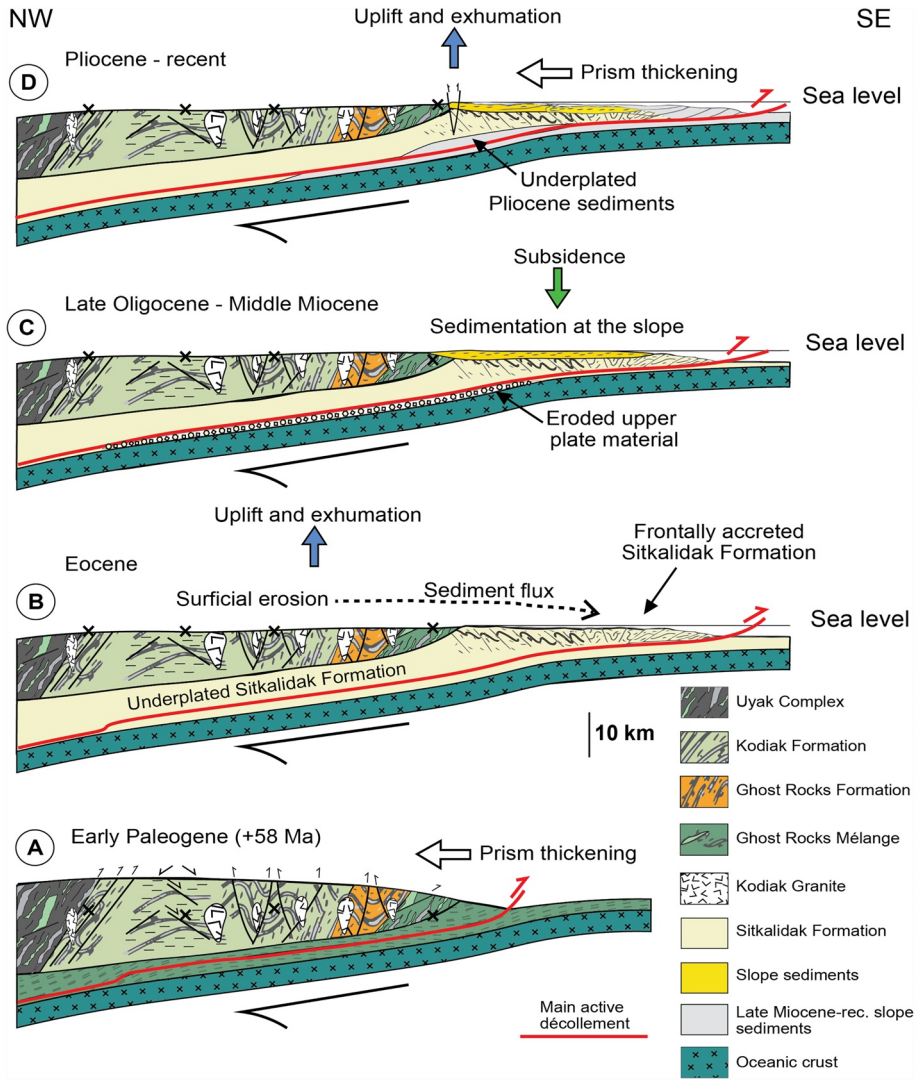


**Figure 15.** Cross-section of the Kodiak accretionary complex evolution with three stages of vertical motion: (a) basal accretion during late Cretaceous-Early Paleogene and associated deformation structures. (b) Exhumation of accreted units by underplating of thick Eocene strata (Moore & Allwardt, 1980). The uplift is coeval with the surficial erosion and exposure of deeply accreted units to their nearly present position. (c) Subsidence recorded in slope sediments in the frontal part of the prism, possibly due to basal erosion. (d) Exhumation of the frontal part of the complex. The recent profile is created based on seismic profiles (M. A. Fisher & Holmes, 1980; von Huene et al., 2012) and onshore observations (Carver et al., 2013; Ramos et al., 2022).

The results from both localities, the Shimanto Belt and the Kodiak complex are evidence of vigorous vertical motion within the prisms, which are not completely understood.

All deformation structures observed during this study are interpreted as forming along the plate-boundary interface or as intra-wedge deformation resulting mainly in the presence horizontal shortening. Overall, we propose that the rock exhumation results from the combination of basal accretion, horizontal shortening, and surficial erosion. In contrast, periods of subsidence evidenced by slope sediments may coincide with basal erosion or result from differential vertical motion across active thrust faults.

## 6. Conclusions

This work provides new insight into vertical motions across the Kodiak accretionary complex using a combination of RSCM temperatures, deformation structures, and relative chronology. The deformation kinematics

of observed structures in all units correspond principally to plane strain in the NW-SE direction from the Early Cretaceous to the present. Simple shear is present in tectonic mélanges and in the Kodiak Formation close to the Uganik Thrust, formed during underthrusting. Conversely, in the coherent units, pure shear is dominant (the Kodiak Seaward Belt and the Ghost Rocks Formation) and results from intra-wedge horizontal shortening. Additional deformation structures are strike-slip faults which postdate the main magmatic event at 58–59 Ma, and vertical shortening in the Kodiak Central Belt for which the timing is still unclear.

Our regional RSCM study across the Kodiak accretionary complex shows temperatures ranging from 220 to 400°C, without discontinuities across unit-bounding faults. The highest temperatures are measured in the Kodiak Central and Seaward Belts, constituting the complex's central portion.

A gap in peak-metamorphic temperatures between accreted units and slope sediments suggests vigorous vertical motion within the wedge between the Paleogene and the Miocene. The period of exhumation of Cretaceous-Paleogene sedimentary units is related to the underplating of younger material, and the lack of significant extensional features indicates that the exhumation occurred due to horizontal shortening and surficial erosion. Later, a following stage of subsidence in the Miocene could be the result of upper crustal faulting and/or a transition from basal accretion to subduction erosion. Estimated rates for this vertical motion are comparable with estimates from other paleo-accretionary prisms.

## Data Availability Statement

Detailed data about sample locations, observed micro- and mesostructures, stress regime, and RSCM temperatures are available at Rajič, Raimbourg, Famin, et al. (2023, https://doi.org/10.5281/zenodo.10004354).

**Acknowledgments**
We thank Old Harbor Native Corporation, Dodge and Danelsky families for the support during the field survey, S. Janiec for the preparation of thin sections and A. Menant for fruitful discussion. We would also like to express our gratitude to P. Vannucchi, W. Behr, and an anonymous reviewer for their valuable suggestions, which have significantly improved this work. Additionally, we appreciate editorial handling by M. Rusmore and F. Rossetti. The authors acknowledge support from LabEx VOLTAIRE (ANR-10-LABX-100-01) and EquipEx PLANEX (ANR-11-EQPX-0036) projects.

## References

Agard, P., Yamato, P., Jolivet, L., & Burov, E. (2009). Exhumation of oceanic blueschists and eclogites in subduction zones: Timing and mechanisms. *Earth-Science Reviews*, *92*(1–2), 53–79. https://doi.org/10.1016/j.earscirev.2008.11.002

Ammar, M. R., & Rouzaud, J.-N. (2012). How to obtain a reliable structural characterization of polished graphitized carbons by Raman microspectroscopy. *Journal of Raman Spectroscopy*, *43*(2), 207–211. https://doi.org/10.1002/jrs.3014

Angiboust, S., Menant, A., Gerya, T., & Oncken, O. (2021). The rise and demise of deep accretionary wedges: A long-term field and numerical modeling perspective. *Geosphere*, *18*(1), 69–103. https://doi.org/10.1130/GES02392.1

Aoya, M., Kouketsu, Y., Endo, S., Shimizu, H., Mizukami, T., Nakamura, D., & Wallis, S. (2010). Extending the applicability of the Raman carbonaceous-material geothermometer using data from contact metamorphic rocks: Raman carbonaceous-material geothermometer. *Journal of Metamorphic Geology*, *28*(9), 895–914. https://doi.org/10.1111/j.1525-1314.2010.00896.x

Arkle, J. C., Armstrong, P. A., Haeussler, P. J., Prior, M. G., Hartman, S., Sendziak, K. L., & Brush, J. A. (2013). Focused exhumation in the syntaxis of the western Chugach Mountains and Prince William Sound, Alaska. *Geological Society of America Bulletin*, *125*(5–6), 776–793. https://doi.org/10.1130/B30738.1

Ascione, A., Ciarcia, S., Di Donato, V., Mazzoli, S., & Vitale, S. (2012). The Pliocene-Quaternary wedge-top basins of southern Italy: An expression of propagating lateral slab tear beneath the Apennines. *Basin Research*, *24*(4), 456–474. https://doi.org/10.1111/j.1365-2117.2011.00534.x

Beyssac, O., Goffé, B., Chopin, C., & Rouzaud, J. N. (2002). Raman spectra of carbonaceous material in metasediments: A new geothermometer. *Journal of Metamorphic Geology*, *20*(9), 859–871. https://doi.org/10.1046/j.1525-1314.2002.00408.x

Beyssac, O., Pattison, D. R. M., & Bourdelle, F. (2019). Contrasting degrees of recrystallization of carbonaceous material in the Nelson aureole, British Columbia and Ballachulish aureole, Scotland, with implications for thermometry based on Raman spectroscopy of carbonaceous material. *Journal of Metamorphic Geology*, *37*(1), 71–95. https://doi.org/10.1111/jmg.12449

Bradley, D. C., Kusky, T. M., Haeussler, P. J., Goldfarb, R. J., Miller, M. L., Dumoulin, J. A., et al. (2003). Geologic signature of early Tertiary ridge subduction in Alaska. In V. B. Sisson, S. M. Roeske, & T. L. Pavlis (Eds.), *Geology of a transpressional orogen developed during ridge-trench interaction along the North Pacific margin*. Geological Society of America. https://doi.org/10.1130/0-8137-2371-X.19

Brandon, M. T., Roden-Tice, M. K., & Garver, J. I. (1998). Late Cenozoic exhumation of the Cascadia accretionary wedge in the Olympic Mountains, northwest Washington State. *Geological Society of America Bulletin*, *110*(8), 985–1009. https://doi.org/10.1130/0016-7606(1998)110<0985:LCEOTC>2.3.CO;2

Brantley, S. L., & Fisher, D. M. (1997). Segregation veins: Evidence for the deformation and dewatering of a low-grade metapelite. In *Deformation-enhanced fluid transport in the Earth's crust and mantle* (pp. 267–288). Chapman & Hall.

Breeding, C. M., & Ague, J. J. (2002). Slab-derived fluids and quartz-vein formation in an accretionary prism, Otago Schist, New Zealand. *Geology*, *30*(6), 499–502. https://doi.org/10.1130/0091-7613(2002)030<0499:sdfaqv>2.0.co;2

Byrne, T. (1982). Structural evolution of coherent terranes in the Ghost Rocks Formation, Kodiak Island, Alaska. *Geological Society, London, Special Publications*, *10*(1), 229–242. https://doi.org/10.1144/GSL.SP.1982.010.01.15

Byrne, T. (1986). Eocene underplating along the Kodiak shelf, Alaska: Implications and regional correlations. *Tectonics*, *5*(3), 403–421. https://doi.org/10.1029/TC005i003p00403

Byrne, T., & Fisher, D. M. (1987). Episodic growth of the Kodiak convergent margin. *Nature*, *325*(6102), 338–341. https://doi.org/10.1038/325338a0

Carver, G., Sauber, J., Lettis, W., Witter, R., & Whitney, B. (2013). Active faults on northeastern Kodiak Island, Alaska. In J. T. Freymueller, P. J. Haeussler, R. L. Wesson, & G. Ekström (Eds.), *Geophysical Monograph Series* (pp. 167–184). American Geophysical Union. https://doi.org/10.1029/179GM09

Ciarcia, S., & Vitale, S. (2013). Sedimentology, stratigraphy and tectonics of evolving wedge-top depozone: Ariano Basin, southern Apennines, Italy. *Sedimentary Geology*, *290*, 27–46. https://doi.org/10.1016/j.sedgeo.2013.02.015

Clendenen, W. S., Fisher, D. M., & Byrne, T. (2003). Cooling and exhumation history of the Kodiak accretionary prism, southwest Alaska. In V. B. Sisson, S. M. Roeske, & T. L. Pavlis (Eds.), *Geology of a transpressional orogen developed during ridge-trench interaction along the North Pacific margin*. Geological Society of America. https://doi.org/10.1130/0-8137-2371-X.71

Clift, P., & Vannucchi, P. (2004). Controls on tectonic accretion versus erosion in subduction zones: Implications for the origin and recycling of the continental crust. *Reviews of Geophysics*, *42*(2), RG2001. https://doi.org/10.1029/2003RG000127

Clift, P. D., Pavlis, T., DeBari, S. M., Draut, A. E., Rioux, M., & Kelemen, P. B. (2005). Subduction erosion of the Jurassic Talkeetna-Bonanza arc and the Mesozoic accretionary tectonics of western North America. *Geology*, *33*(11), 881. https://doi.org/10.1130/G21822.1

Connelly, W. (1978). Uyak complex, Kodiak Islands, Alaska: A Cretaceous subduction complex. *Geological Society of America Bulletin*, *89*(5), 755–769. https://doi.org/10.1130/0016-7606(1978)89<755:uckiaa>2.0.co;2

Corrado, S., Aldega, L., Perri, F., Critelli, S., Muto, F., Schito, A., & Tripodi, V. (2019). Detecting syn-orogenic extension and sediment provenance of the Cilento wedge top basin (southern Apennines, Italy): Mineralogy and geochemistry of fine-grained sediments and petrography of dispersed organic matter. *Tectonophysics*, *750*, 404–418. https://doi.org/10.1016/j.tecto.2018.10.027

Dahlen, F. A. (1984). Noncohesive critical Coulomb wedges: An exact solution. *Journal of Geophysical Research*, *89*(B12), 10125–10133. https://doi.org/10.1029/JB089iB12p10125

Dahlen, F. A. (1990). Critical taper model of fold-and-thrust belts and accretionary wedges. *Annual Review of Earth and Planetary Sciences*, *18*(1), 55–99. https://doi.org/10.1146/annurev.ea.18.050190.000415

Davis, D., Suppe, J., & Dahlen, F. A. (1983). Mechanics of fold-and-thrust belts and accretionary wedges. *Journal of Geophysical Research*, *88*(B2), 1153–1172. https://doi.org/10.1029/JB088iB02p01153

Delchini, S., Lahfid, A., Plunder, A., & Michard, A. (2016). Applicability of the RSCM geothermometry approach in a complex tectono-metamorphic context: The Jebilet massif case study (Variscan Belt, Morocco). *Lithos*, *256–257*, 1–12. https://doi.org/10.1016/j.lithos.2016.04.007

DeLong, S. E., Schwarz, W. M., & Anderson, R. N. (1979). Thermal effects of ridge subduction. *Earth and Planetary Science Letters*, *44*(2), 239–246. https://doi.org/10.1016/0012-821X(79)90172-9

Delvaux, D., Kipata, L., & Sintubin, M. (2013). Tectonic stress inversion of large multi-phase fracture data sets: Application of Win-Tensor to reveal the brittle tectonic history of the Lufilan Arc, DRC. In *EGU General Assembly 2013* (Vol. 15, p. 1).

Delvaux, D., & Sperner, B. (2003). New aspects of tectonic stress inversion with reference to the TENSOR program. *Geological Society, London, Special Publications*, *212*(1), 75–100. https://doi.org/10.1144/GSL.SP.2003.212.01.06

Ernst, W. G., & McLaughlin, R. J. (2012). Mineral parageneses, regional architecture, and tectonic evolution of Franciscan metagraywackes, Cape Mendocino-Garberville-Covelo 30′ × 60′ quadrangles, northwest California. *Tectonics*, *31*(1), TC1001. https://doi.org/10.1029/2011TC002987

Fagereng, Å., & Sibson, R. H. (2010). Mélange rheology and seismic style. *Geology*, *38*(8), 751–754. https://doi.org/10.1130/G30868.1

Farris, D. W. (2010). Tectonic and petrologic evolution of the Kodiak batholith and the trenchward belt, Kodiak Island, AK: Contact fault juxtaposition? *Journal of Geophysical Research*, *115*(B7), B07208. https://doi.org/10.1029/2009JB006434

Farris, D. W., & Haeussler, P. J. (2020). *Selected Geologic Maps of the Kodiak Batholith and Other Paleocene Intrusive Rocks, Kodiak Island, Alaska: U.S. Geological Survey Scientific Investigations Map 3441 (pamphlet 10 p., scale 1:50,000)*. USGS.

Farris, D. W., Haeussler, P. J., Friedman, R., Paterson, S. R., Saltus, R. W., & Ayuso, R. (2006). Emplacement of the Kodiak batholith and slab-window migration. *Geological Society of America Bulletin*, *118*(11–12), 1360–1376. https://doi.org/10.1130/B25718.1

Farris, D. W., & Paterson, S. R. (2009). Subduction of a segmented ridge along a curved continental margin: Variations between the western and eastern Sanak–Baranof belt, southern Alaska. *Tectonophysics*, *464*(1–4), 100–117. https://doi.org/10.1016/j.tecto.2007.10.008

Fisher, D. M., Brantley, S. L., Everett, M., & Dzvonik, J. (1995). Cyclic fluid flow through a regionally extensive fracture network within the Kodiak accretionary prism. *Journal of Geophysical Research*, *100*(B7), 12881–12894. https://doi.org/10.1029/94JB02816

Fisher, D. M., & Byrne, T. (1987). Structural evolution of underthrusted sediments, Kodiak Islands, Alaska. *Tectonics*, *6*(6), 775–793. https://doi.org/10.1029/TC006i006p00775

Fisher, D. M., & Byrne, T. (1990). The character and distribution of mineralized fractures in the Kodiak Formation, Alaska: Implications for fluid flow in an Underthrust sequence. *Journal of Geophysical Research*, *95*(B6), 9069–9080. https://doi.org/10.1029/JB095iB06p09069

Fisher, D. M., & Byrne, T. (1992). Strain variations in an ancient accretionary complex: Implications for forearc evolution. *Tectonics*, *11*(2), 330–347. https://doi.org/10.1029/91TC01490

Fisher, D. M., Tonai, S., Hashimoto, Y., Tomioka, N., & Oakley, D. (2019). K-Ar dating of fossil seismogenic thrusts in the Shimanto accretionary complex, southwest Japan. *Tectonics*, *38*(11), 3866–3880. https://doi.org/10.1029/2019TC005571

Fisher, M. A. (1979). Structure and tectonic setting of continental shelf southwest of Kodiak Island, Alaska. *AAPG Bulletin*, *63*, 301–310. https://doi.org/10.1306/C1EA55FD-16C9-11D7-8645000102C1865D

Fisher, M. A. (1980). Petroleum geology of Kodiak shelf, Alaska. *AAPG Bulletin*, *64*(8), 1140–1157.

Fisher, M. A., & Holmes, M. L. (1980). Large-scale structure of deep strata beneath Kodiak shelf, Alaska. *Geological Society of America Bulletin*, *91*(4), 218–224. https://doi.org/10.1130/0016-7606(1980)91<218:LSODSB>2.0.CO;2

Forster, M. A., & Lister, G. S. (2003). Cretaceous metamorphic core complexes in the Otago Schist, New Zealand. *Australian Journal of Earth Sciences*, *50*(2), 181–198. https://doi.org/10.1046/j.1440-0952.2003.00986.x

Guillot, S., Hattori, K., Agard, P., Schwartz, S., & Vidal, O. (2009). Exhumation processes in oceanic and continental subduction contexts: A review. In S. Lallemand & F. Funiciello (Eds.), *Subduction zone geodynamics* (pp. 175–205). Springer Berlin Heidelberg. https://doi.org/10.1007/978-3-540-87974-9_10

Hilchie, L. J., & Jamieson, R. A. (2014). Graphite thermometry in a low-pressure contact aureole, Halifax, Nova Scotia. *Lithos*, *208–209*, 21–33. https://doi.org/10.1016/j.lithos.2014.08.015

Katagiri, G., Ishida, H., & Ishitani, A. (1988). Raman spectra of graphite edge planes. *Carbon*, *26*(4), 565–571. https://doi.org/10.1016/0008-6223(88)90157-1

Kondo, H., Kimura, G., Masago, H., Ohmori-Ikehara, K., Kitamura, Y., Ikesawa, E., et al. (2005). Deformation and fluid flow of a major out-of-sequence thrust located at seismogenic depth in an accretionary complex: Nobeoka Thrust in the Shimanto Belt, Kyushu, Japan. *Tectonics*, *24*(6), TC6008. https://doi.org/10.1029/2004TC001655

Kulm, L. D., von Huene, R., Duncan, J. R., Ingle, J. C., Jr., Kling, S. A., Musich, L. F., et al. (1973). *Initial Reports of the Deep Sea Drilling Project* (Vol. 18). U.S. Government Printing Office. https://doi.org/10.2973/dsdp.proc.18.1973

Lahfid, A., Beyssac, O., Deville, E., Negro, F., Chopin, C., & Goffé, B. (2010). Evolution of the Raman spectrum of carbonaceous material in low-grade metasediments of the Glarus Alps (Switzerland): RSCM in low-grade metasediments. *Terra Nova*, *22*(5), 354–360. https://doi.org/10.1111/j.1365-3121.2010.00956.x

Menant, A., Angiboust, S., Gerya, T., Lacassin, R., Simoes, M., & Grandin, R. (2020). Transient stripping of subducting slabs controls periodic forearc uplift. *Nature Communications*, *11*(1), 1823. https://doi.org/10.1038/s41467-020-15580-7

Meneghini, F., Marroni, M., Moore, J. C., Pandolfi, L., & Rowe, C. D. (2009). The processes of underthrusting and underplating in the geologic record: Structural diversity between the Franciscan Complex (California), the Kodiak Complex (Alaska) and the Internal Ligurian Units (Italy). *Geological Journal*, *44*(2), 126–152. https://doi.org/10.1002/gj.1144

Moore, G. F., Taira, A., Klaus, A., Becker, L., Boeckel, B., Cragg, B. A., et al. (2001). New insights into deformation and fluid flow processes in the Nankai Trough accretionary prism: Results of Ocean Drilling Program Leg 190. *Geochemistry, Geophysics, Geosystems*, *2*(10), 1058. https://doi.org/10.1029/2001GC000166

Moore, J. C. (1978). Orientation of underthrusting during latest Cretaceous and earliest Tertiary time, Kodiak Islands, Alaska. *Geology*, *6*(4), 209–213. https://doi.org/10.1130/0091-7613(1978)6<209:ooudlc>2.0.co;2

Moore, J. C. (1989). Tectonics and hydrogeology of accretionary prisms: Role of the décollement zone. *Journal of Structural Geology*, *11*(1–2), 95–106. https://doi.org/10.1016/0191-8141(89)90037-0

Moore, J. C., & Allwardt, A. (1980). Progressive deformation of a Tertiary Trench Slope, Kodiak Islands, Alaska. *Journal of Geophysical Research*, *85*(B9), 4741–4756. https://doi.org/10.1029/jb085ib09p04741

Moore, J. C., Byrne, T., Plumley, P. W., Reid, M., Gibbons, H., & Coe, R. S. (1983). Paleogene evolution of the Kodiak Islands, Alaska: Consequences of ridge-trench interaction in a more southerly latitude. *Tectonics*, *2*(3), 265–293. https://doi.org/10.1029/tc002i003p00265

Moore, J. C., Diebold, J., Fisher, M. A., Sample, J., Brocher, T., Talwani, M., et al. (1991). EDGE deep seismic reflection transect of the eastern Aleutian arc-trench layered lower crust reveals underplating and continental growth. *Geology*, *19*(5), 420. https://doi.org/10.1130/0091-7613(1991)019<0420:EDSRTO>2.3.CO;2

Moore, J. C., Mascle, A., Taylor, E., & Underwood, M. B. (1990). In *Proceedings of the Ocean Drilling Program*, *Scientific Results* (Vol. 110). Ocean Drilling Program. https://doi.org/10.2973/odp.proc.sr.110.1990

Morell, K. D., Fisher, D. M., & Bangs, N. (2019). Plio-Quaternary outer forearc deformation and Mass balance of the southern Costa Rica convergent margin. *Journal of Geophysical Research: Solid Earth*, *124*(9), 9795–9815. https://doi.org/10.1029/2019JB017986

Mori, N., Wallis, S., & Mori, H. (2015). Graphitization of carbonaceous material in sedimentary rocks on short geologic time-scales: An example from the Kinsho-zan area, central Japan. *Island Arc*, *24*(2), 119–130. https://doi.org/10.1111/iar.12093

Mortimer, N. (2000). Metamorphic discontinuities in orogenic belts: Example of the garnet-biotite-albite zone in the Otago Schist, New Zealand. *International Journal of Earth Sciences*, *89*(2), 295–306. https://doi.org/10.1007/s005310000086

Müller, R. D., Sdrolias, M., Gaina, C., Steinberger, B., & Heine, C. (2008). Long-term sea-level fluctuations driven by ocean basin dynamics. *Science*, *319*(5868), 1357–1362. https://doi.org/10.1126/science.1151540

Myers, G., & Vrolijk, P. (1986). Fluid evolution associated with the accretion of the Kodiak Formation, Kodiak Island, Alaska. *Eos, Transactions American Geophysical Union*, *67*, 1219.

Noda, A., & Miyakawa, A. (2017). Deposition and deformation of modern accretionary-type forearc basins: Linking basin formation and accretionary wedge growth. In Y. Itoh (Ed.), *Evolutionary models of convergent margins—Origin of their diversity*. InTech. https://doi.org/10.5772/67559

Osozawa, S., & Wakabayashi, J. (2015). Late stage exhumation of HP metamorphic rocks, progressive localization of strain, and changes in transport direction, Sambagawa belt, Japan. *Journal of Structural Geology*, *75*, 1–16. https://doi.org/10.1016/j.jsg.2015.03.006

Pajang, S., Cubas, N., Letouzey, J., Le Pourhiet, L., Seyedali, S., Fournier, M., et al. (2021). Seismic hazard of the western Makran subduction zone: Insight from mechanical modelling and inferred frictional properties. *Earth and Planetary Science Letters*, *562*, 116789. https://doi.org/10.1016/j.epsl.2021.116789

Palazzin, G., Raimbourg, H., Famin, V., Jolivet, L., Kusaba, Y., & Yamaguchi, A. (2016). Deformation processes at the down-dip limit of the seismogenic zone: The example of Shimanto accretionary complex. *Tectonophysics*, *687*, 28–43. https://doi.org/10.1016/j.tecto.2016.08.013

Pasteris, J. D. (1989). In situ analysis in geological thin-sections by laser Raman microprobe spectroscopy: A cautionary note. *Applied Spectroscopy*, *43*(3), 567–570. https://doi.org/10.1366/0003702894202878

Pavlis, T. L., Monteverde, D. H., Bowman, J. R., Rubenstone, J. L., & Reason, M. D. (1988). Early Cretaceous near-trench plutonism in southern Alaska: Atonalite-Trondhjemite Intrusive Complex injected during ductile thrusting along the Border Ranges Fault System. *Tectonics*, *7*(6), 1179–1199. https://doi.org/10.1029/TC007i006p01179

Petroccia, A., Carosi, R., Montomoli, C., Iaccarino, S., & Vitale Brovarone, A. (2022). Deformation and temperature variation along thrust-sense shear zones in the hinterland-foreland transition zone of collisional settings: A case study from the Barbagia thrust (Sardinia, Italy). *Journal of Structural Geology*, *161*, 104640. https://doi.org/10.1016/j.jsg.2022.104640

Plafker, G., Moore, J. C., & Winkler, G. R. (1994). Geology of the southern Alaska margin. In G. Plafker & H. C. Berg (Eds.), *The Geology of Alaska* (Vol. 1, pp. 389–449). Geological Society of America.

Platt, J. P. (1986). Dynamics of orogenic wedges and the uplift of high-pressure metamorphic rocks. *Geological Society of America Bulletin*, *97*(9), 1037–1093. https://doi.org/10.1130/0016-7606(1986)97<1037:doowat>2.0.co;2

Raimbourg, H., Augier, R., Famin, V., Gadenne, L., Palazzin, G., Yamaguchi, A., & Kimura, G. (2014). Long-term evolution of an accretionary prism: The case study of the Shimanto Belt, Kyushu, Japan. *Tectonics*, *33*(6), 936–959. https://doi.org/10.1002/2013TC003412

Raimbourg, H., Famin, V., Palazzin, G., Yamaguchi, A., & Augier, R. (2017). Tertiary evolution of the Shimanto belt (Japan): A large-scale collision in Early Miocene. *Tectonics*, *36*(7), 1317–1337. https://doi.org/10.1002/2017TC004529

Raimbourg, H., Famin, V., Palazzin, G., Yamaguchi, A., Augier, R., Kitamura, Y., & Sakaguchi, A. (2019). Distributed deformation along the subduction plate interface: The role of tectonic mélanges. *Lithos*, *334*, 69–87. https://doi.org/10.1016/j.lithos.2019.01.033

Rajič, K., Raimbourg, H., Famin, V., Moris-Muttoni, B., Fisher, D., Morell, K., & Canizarés, A. (2023). Structural analysis and peak-metamorphic temperatures across the Kodiak accretionary complex [Dataset]. Zenodo. https://doi.org/10.5281/zenodo.10004354

Rajič, K., Raimbourg, H., Lerouge, C., Famin, V., Dubacq, B., Canizarès, A., et al. (2023). Metamorphic reactions and their implication for the fluid budget in metapelites at seismogenic depths in subduction zones. *Tectonophysics*, *857*, 229844. https://doi.org/10.1016/j.tecto.2023.229844

Ramos, M. D., Liberty, L. M., Haeussler, P. J., & Humphreys, R. (2022). Upper-plate structure and tsunamigenic faults near the Kodiak Islands, Alaska, USA. *Geosphere*, *18*(5), 1474–1491. https://doi.org/10.1130/GES02486.1

Ring, U., Brandon, M. T., Willett, S. D., & Lister, G. S. (1999). Exhumation processes. *Geological Society, London, Special Publications*, *154*(1), 1–27. https://doi.org/10.1144/GSL.SP.1999.154.01.01

Roeske, S. M., Mattinson, J. M., & Armstrong, R. L. (1989). Isotopic ages of glaucophane schists on the Kodiak Islands, southern Alaska, and their implications for the Mesozoic tectonic history of the Border Ranges fault system. *Geological Society of America Bulletin*, *101*(8), 1021–1037. https://doi.org/10.1130/0016-7606(1989)101<1021:iaogso>2.3.co;2

Rowe, C. D., Meneghini, F., & Moore, J. C. (2009). Fluid-rich damage zone of an ancient out-of-sequence thrust, Kodiak Islands, Alaska. *Tectonics*, *28*(1), TC1006. https://doi.org/10.1029/2007TC002126

Sakaguchi, A. (1999). Thermal maturity in the Shimanto accretionary prism, southwest Japan, with the thermal change of the subducting slab: Fluid inclusion and vitrinite reflectance study. *Earth and Planetary Science Letters*, *173*(1–2), 61–74. https://doi.org/10.1016/S0012-821X(99)00219-8

Sample, J. C., & Fisher, D. M. (1986). Duplex accretion and underplating in an ancient accretionary prism, Kodiak Islands, Alaska. *Geology*, *14*(2), 160–163. https://doi.org/10.1130/0091-7613(1986)14<160:daauia>2.0.co;2

Sample, J. C., & Moore, J. C. (1987). Structural style and kinematics of an underplated slate belt, Kodiak and adjacent islands, Alaska. *Geological Society of America Bulletin*, *99*(1), 7–20. https://doi.org/10.1130/0016-7606(1987)99<7:ssakoa>2.0.co;2

Schito, A., Corrado, S., Aldega, L., & Grigo, D. (2016). Overcoming pitfalls of vitrinite reflectance measurements in the assessment of thermal maturity: The case history of the lower Congo basin. *Marine and Petroleum Geology*, *74*, 59–70. https://doi.org/10.1016/j.marpetgeo.2016.04.002

Schito, A., Romano, C., Corrado, S., Grigo, D., & Poe, B. (2017). Diagenetic thermal evolution of organic matter by Raman spectroscopy. *Organic Geochemistry*, *106*, 57–67. https://doi.org/10.1016/j.orggeochem.2016.12.006

Smeraglia, L., Aldega, L., Billi, A., Carminati, E., Di Fiore, F., Gerdes, A., et al. (2019). Development of an intrawedge tectonic mélange by out-of-sequence thrusting, buttressing, and intraformational rheological contrast, Mt. Massico ridge, Apennines, Italy. *Tectonics*, *38*(4), 1233–1249. https://doi.org/10.1029/2018TC005243

Sperner, B., & Zweigel, P. (2010). A plea for more caution in fault–slip analysis. *Tectonophysics*, *482*(1–4), 29–41. https://doi.org/10.1016/j.tecto.2009.07.019

Tagami, T., & Dumitru, T. A. (1996). Provenance and thermal history of the Franciscan accretionary complex: Constraints from zircon fission track thermochronology. *Journal of Geophysical Research*, *101*(B5), 11353–11364. https://doi.org/10.1029/96JB00407

Toriumi, M., & Teruya, J. (1988). Tectono-metamorphism of the Shimanto Belt. *Modern Geology*, *12*, 303–324.

von Huene, R., Miller, J. J., & Weinrebe, W. (2012). Subducting plate geology in three great earthquake ruptures of the western Alaska margin, Kodiak to Unimak. *Geosphere*, *8*(3), 628–644. https://doi.org/10.1130/GES00715.1

Vrolijk, P., Myers, G., & Moore, J. C. (1988). Warm fluid migration along tectonic melanges in the Kodiak Accretionary Complex, Alaska. *Journal of Geophysical Research*, *93*(B9), 10313–10324. https://doi.org/10.1029/JB093iB09p10313

Wakabayashi, J. (2015). Anatomy of a subduction complex: Architecture of the Franciscan Complex, California, at multiple length and time scales. *International Geology Review*, *57*(5–8), 669–746. https://doi.org/10.1080/00206814.2014.998728

Weinberger, J., & Sisson, V. B. (2003). Pressure and temperature conditions of brittle-ductile vein emplacement in the greenschist facies, Chugach metamorphic complex, Alaska: Evidence from fluid inclusions. In V. B. Sisson, S. M. Roeske, & T. L. Pavlis (Eds.), *Geology of a transpressional orogen developed during ridge-trench interaction along the North Pacific margin*. Geological Society of America. https://doi.org/10.1130/0-8137-2371-X.217

Wilson, F. H., Labay, K. A., Mohadjer, S., & Shew, N. (2005). Preliminary integrated geologic map databases for the United States—Digital data for the reconnaissance geologic map for the Kodiak Islands, Alaska [geologic map compiled by F.H. Wilson], *U.S. Geological Survey Open-File Report 2005–1340*. Retrieved from https://pubs.usgs.gov/of/2005/1340/

Yamato, P., Burov, E., Agard, P., Le Pourhiet, L., & Jolivet, L. (2008). HP-UHP exhumation during slow continental subduction: Self-consistent thermodynamically and thermomechanically coupled model with application to the Western Alps. *Earth and Planetary Science Letters*, *271*(1–4), 63–74. https://doi.org/10.1016/j.epsl.2008.03.049